

Photodynamic Therapy

DNA Intercalating Ru^{II} Polypyridyl Complexes as Effective Photosensitizers in Photodynamic Therapy

Cristina Mari,^[a] Vanessa Pierroz,^[a, b] Riccardo Rubbiani,^[a] Malay Patra,^[a] Jeannine Hess,^[a] Bernhard Spingler,^[a] Luciano Oehninger,^[c] Julia Schur,^[c] Ingo Ott,^[c] Luca Salassa,^[d, e] Stefano Ferrari,^[b] and Gilles Gasser*^[a]

Abstract: Six substitutionally inert [Ru^{II}(bipy)₂dppz]²⁺ derivatives (bipy = 2,2'-bipyridine, dppz = dipyrido[3,2-a:2',3'-c]phenazine) bearing different functional groups on the dppz ligand [NH₂ (**1**), OMe (**2**), OAc (**3**), OH (**4**), CH₂OH (**5**), CH₂Cl (**6**)] were synthesized and studied as potential photosensitizers (PSs) in photodynamic therapy (PDT). As also confirmed by DFT calculations, all complexes showed promising ¹O₂ production quantum yields, well comparable with PSs available on the market. They can also efficiently intercalate into the DNA double helix, which is of high interest in view of DNA targeting. The cellular localization and uptake quantification of **1–6** were assessed by confocal microscopy and high-resolution continuum source atomic absorption spec-

troscopy. Compound **1**, and especially **2**, showed very good uptake in cervical cancer cells (HeLa) with preferential nuclear accumulation. None of the compounds studied was found to be cytotoxic in the dark on both HeLa cells and, interestingly, on noncancerous MRC-5 cells (IC₅₀ > 100 μM). However, **1** and **2** showed very promising behavior with an increment of about 150 and 42 times, respectively, in their cytotoxicities upon light illumination at 420 nm in addition to a very good human plasma stability. As anticipated, the preferential nuclear accumulation of **1** and **2** and their very high DNA binding affinity resulted in very efficient DNA photocleavage, suggesting a DNA-based mode of phototoxic action.

Introduction

Photodynamic therapy (PDT) is a medical technique which is currently approved and used in several countries for the treatment of dermatological diseases and some types of cancer.^[1–4] PDT is based on the combination of a photoactive compound and light to induce cell death using an oxygen-dependent mechanism. More specifically, a (preferably nontoxic) photo-

sensitizer (PS) is irradiated with light at a certain wavelength to achieve its excitation to a triplet state. The excited PS can then transfer electrons or protons to the close substrates to form radicals, which can further react with molecular oxygen to generate reactive oxygen species (ROS, type-I reactions). In parallel, the PS is able to transfer its energy to surrounding molecular triplet oxygen (³O₂) leading to the generation of oxygen in its singlet state (¹O₂, type-II reactions).^[2] These two mechanisms can happen simultaneously, but nowadays the type-II mechanism is the predominant pathway for most of the commercially available PSs.^[4] ¹O₂ is a very reactive and toxic form of oxygen, which induces a deep cellular cascade that ultimately leads to cell death. Due to its high reactivity, the half-life of ¹O₂ is very short in cellular environment. PDT therefore offers the possibility to induce cell death with spatial and temporal control, activating the cytotoxic mechanism only in the irradiated area. As a consequence, PDT has gained great interest in the treatment of certain types of cancer due to its selectivity, the low systemic cumulative toxicity of the PSs as well as the possibility of its use in combination with other anticancer therapies. One of the crucial parameters for a successful PDT treatment is the use of an adequate PS. Among the required properties, the PS must have a high phototoxic index (PI = IC₅₀ in the dark/IC₅₀ upon irradiation) and must be activated at a specific wavelength, preferably in the red or near-IR region due to the deeper penetration of light into tissues and its lower harmfulness. Other characteristics of an ideal PS are good chemical, biological and photostability as well as an excellent efficiency in the photo-

[a] C. Mari, V. Pierroz, Dr. R. Rubbiani, Dr. M. Patra, J. Hess, Priv.-Doz. Dr. B. Spingler, Prof. Dr. G. Gasser
Department of Chemistry, University of Zurich
Winterthurerstrasse 190, CH-8057 Zurich (Switzerland)
WWW: www.gassergroup.com
E-mail: gilles.gasser@chem.uzh.ch

[b] V. Pierroz, Priv.-Doz. Dr. S. Ferrari
Institute of Molecular Cancer Research, University of Zurich
Winterthurerstrasse 190, CH-8057 Zurich (Switzerland)

[c] Dr. L. Oehninger, J. Schur, Prof. Dr. I. Ott
Institute of Medicinal and Pharmaceutical Chemistry
Technische Universität Braunschweig
Beethovenstrasse 55, 38106 Braunschweig (Germany)

[d] Dr. L. Salassa
CIC biomaGUNE, Paseo de Miramón 182, 20009
Donostia - San Sebastián (Spain)

[e] Dr. L. Salassa
Kimika Fakultatea, Euskal Herriko Unibertsitatea and
Donostia International Physics Center (DIPC)
P.K. 1072 Donostia, Euskadi (Spain)

Supporting information for this article is available on the WWW under <http://dx.doi.org/10.1002/chem.201402796>.

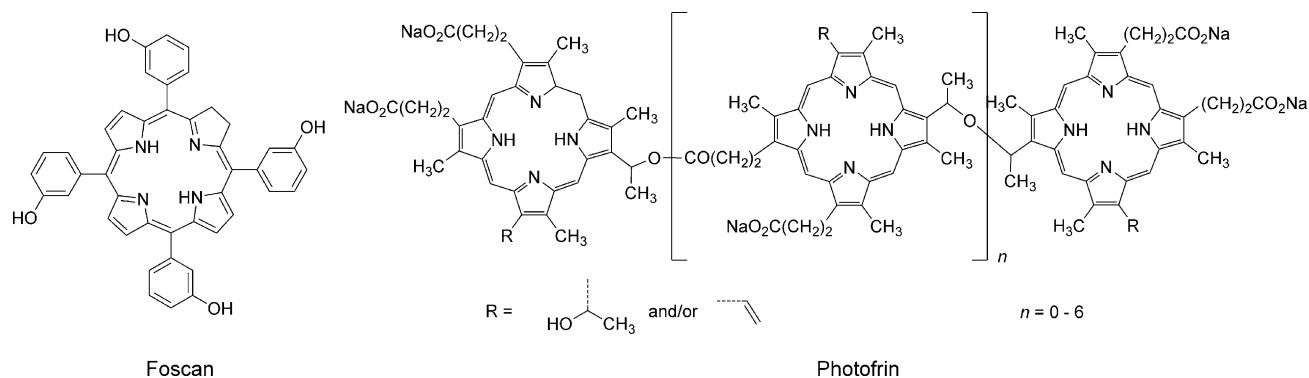
sensitization of molecular oxygen.^[5,6] Porphyrins, chlorins and phthalocyanines are known to preferentially accumulate in cancer cells and to photosensitize molecular oxygen with high yields.^[2,7] Photofrin and Foscan are the most common examples of such PSs (Scheme 1). However, the clinically used PSs suffer generally from several drawbacks such as: 1) tedious synthesis and purification, 2) very low solubility in aqueous media, and 3) slow clearance from the body in some cases, thus leading to prolonged light sensitivity (even ten weeks after treatment with Photofrin). Great efforts have therefore been devoted to the search for structurally new classes of PSs or on the structural modification of existing ones.^[8–16]

The biological activity of ruthenium complexes is known since decades.^[17–20] NAMI-A and KP1339 (the sodium salt of KP1019) are the two most prominent examples of Ru-based anticancer agents since they are currently undergoing clinical trials.^[21–25] With the view of achieving multimodal activity, Ru-arene anticancer complexes were conjugated to porphyrin PSs by Therrien and co-workers.^[26] The authors showed that their Ru-porphyrin systems were effective PSs at a light dose of 5 J cm^{-2} at 652 nm. More recently, Alessio et al.^[27] described the preparation of new porphyrin systems derivatized with one bipyridyl ligand suitable for Ru complexation. Three of these compounds showed interesting phototoxic activity, becoming ten-times more toxic upon light irradiation at 590–700 nm (from low micromolar concentration in the dark to nanomolar concentration with light doses between 1 and 10 J cm^{-2}). Coordinatively saturated and substitutionally inert ruthenium(II) polypyridyl complexes have been intensively studied for their interesting features as DNA intercalating probes^[28–30] and also recently as cytotoxic agents.^[20,31–38] Kwong et al. recently reported the preparation and biological evaluation of a series of Ru polypyridyl-porphyrin conjugates as bifunctional tumor imaging and PDT agents.^[39–41] A phototoxicity of $1 \mu\text{M}$ was obtained for a few of their compounds when yellow light was applied (500–600 nm) at different doses (from 2 to 11.5 J cm^{-2}). A correlation between the localization of the conjugates (cytoplasm, mitochondria and lysosome) and the cell mortality due to $^1\text{O}_2$ induced oxidative damage was also established. During recent years, several Ru complexes with DNA intercalating moieties were studied for their ability to produce ROS upon light irradiation and to consequently

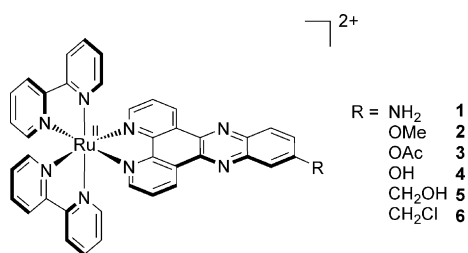
photocleave DNA. However, in most cases, no evaluation of the cellular phototoxicity was performed.^[42–53] To the best of our knowledge, there are only scarce examples of metal complexes which are able to noncovalently interact with DNA (e.g., by intercalation) and which are characterized by photodynamic activity. The combination of these two features can be extremely promising in the design of a PS. This is the case because singlet oxygen, which is responsible for PDT damage, is known to have a very short lifetime. A PS which is tightly bound to DNA will allow the production of the toxic species in the very proximity of the genetic material and the PDT damage to occur with high efficacy.^[54] Of note, Turro et al.^[55] reported dirhodium(II) dppz complexes which are able to intercalate into DNA double helix and exert a phototoxic effect with an increase of cytotoxicity of 3.4-times upon irradiation at 400–700 nm. However, they also highlighted that higher phototoxicity was not correlating with stronger DNA binding affinity. Chakravarty and co-workers^[56] designed ferrocene-conjugated Cu^{II} polypyridyl complexes with good DNA binding affinity ($K_b \sim 10^5 \text{ M}^{-1}$ per nucleotide). In the case of the most active complex, a 2.8-fold increase of cytotoxicity was achieved upon irradiation at 400–700 nm. The mechanism of toxicity seems to be dependent on the production of hydroxy radical ($^{\bullet}\text{OH}$) since the presence of $^{\bullet}\text{OH}$ scavengers inhibits the DNA photocleavage ability of the complex. McFarland recently presented Ru^{II} complexes with a phenanthroline ligand substituted with a pyrenylethynylene moiety that showed impressive phototoxicity upon white-light irradiation. However, the DNA interaction was not thought to play a major role.^[57]

Considering the enormous potential of Ru polypyridyl complexes with strong DNA affinity as PSs in PDT, we recently embarked on a program to investigate the applicability of such compounds in this field of research. In this study, we report on our findings. More specifically, the synthesis and characterization of four novel Ru^{II} bis(bipyridyl)-dipyridophenazine-based complexes (3–6, Scheme 2) is described and, together with the previously reported complexes 1 and 2, an in-depth investigation of the behavior of these compounds as PSs is reported.

Furthermore, compounds 3 and 6 were characterized by X-ray crystallography and a set of DFT calculations was performed for 1–3 and 6 to obtain more insight into their photo-physical properties. The DNA binding affinity upon intercala-



Scheme 1. Structures of commercially available photosensitizers Foscan and Photofrin.



Scheme 2. Structure of the ruthenium complexes. Note that the complexes were synthesized as PF₆⁻ salts and exist as racemic mixtures.

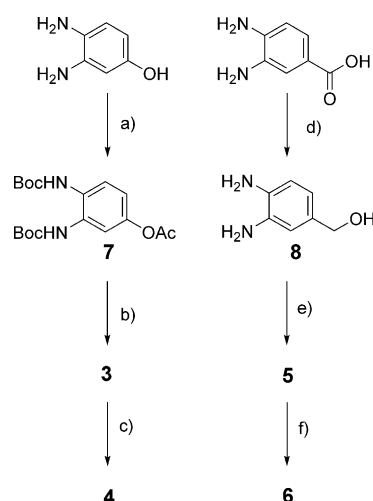
tion (together with the light-switch effect) and the ability to produce singlet oxygen by light excitation are also reported. The cellular localization of 1–6 was studied by confocal microscopy and the cellular uptake of the compounds was quantified by high-resolution continuum source atomic absorption spectrometry (HR-CS AAS). Cytotoxicity on cervical cancer (HeLa) and noncancerous cell (MRC-5) lines of the complexes in the dark and upon light activation at 350 nm as well as 420 nm is also presented. Moreover, the DNA photocleavage ability of the most phototoxic complexes was evaluated to highlight the possible DNA damage induced.

Results and Discussion

Syntheses and characterization of complexes 1–6

The complexes synthesized in this work are listed in Scheme 2. To the best of our knowledge, the synthesis of complexes 3–6 has never been reported while complexes 1^[58,59] and 2^[60] were synthesized as previously described in the literature. The synthetic procedures applied to obtain the desired compounds 3–6 are reported in Scheme 3. For the synthesis of 4, efforts of cleaving the methyl ether of 2 using BBr₃ in CHCl₃ were found to be unsuccessful. Even after 48 h, considerable amount of 2 was still present in the reaction mixture. LC-MS analysis showed the formation of 4 with other unidentified byproducts. This is most likely due to the poor solubility of 2 in CHCl₃. Moreover, the direct condensation of 4-hydroxyphenylenediamine with either phenanthroline^[61] or [Ru(bipy)₂phenanthroline]²⁺^[62] was also found to be not successful. However, 4 was finally obtained using an alternative procedure. 4-Hydroxyphenylenediamine was first Boc protected and the hydroxyl group was then acetylated to give 7. TFA-mediated Boc deprotection of 7, followed by a condensation reaction with [Ru(bipy)₂phenanthroline]²⁺, provided 3 in 65% yield. Complex 3 was then subjected to basic ester hydrolysis to form 4. Structure of 3 was confirmed by X-ray crystallography showing the presence of the acetoxy group on the dppz ligand (Figure 1, see also X-ray crystallography section below). ESI-MS spectra confirmed the successful synthesis of 4 with a peak at *m/z* 356 that corresponds to the [M–2PF₆]²⁺ species. Complexes 5 and 6 were obtained by adapting a procedure used to synthesize the analogous diphenanthroline complexes.^[63] 3,4-Diaminobenzoic acid was converted to the ethyl ester, which was then reduced with LiAlH₄

to the hydroxymethyl derivative 8. A condensation reaction between 8 and [Ru(bipy)₂phenanthroline]²⁺ resulted in the formation of 5. The hydroxyl group was then transformed into a chloride by treatment with oxalyl chloride to give 6. In the ¹H NMR of 5 (Figure S5 in the Supporting Information), protons 6 and 8 (see Chart S1 in the Supporting Information for proton assignment) from the phenazine ring are clearly visible between 8.3 and 8.4 ppm and the CH₂ protons appear at 4.9 ppm. In complex 6 (Figure S7 in the Supporting Information), these protons are shifted to 8.45 and 5.0 ppm, respectively, due to the presence of the more electron-withdrawing chloride. We were able to obtain single crystals of 6 suitable for X-ray crystallography by slow diffusion of a KClO₄ aqueous solution into an acetonitrile solution of 6 as hexafluorophosphate salt (Figure S9 in the Supporting Information, see also X-ray crystallography section below).



Scheme 3. Syntheses of complexes 3–6. Reaction conditions: a) i) Boc₂O, THF; ii) CH₃COCl, NEt₃; b) i) TFA, CH₂Cl₂; ii) [Ru(bipy)₂phenanthroline](PF₆)₂, CH₃CN, EtOH; c) 1 M NaOH, MeOH; d) i) H₂SO₄, EtOH; ii) LiAlH₄, dry THF; e) [Ru(bipy)₂phenanthroline](PF₆)₂, AcOH, CH₃CN; f) (COCl)₂, DMF, CH₃CN; phenanthroline = 1,10-phenanthroline-5,6-dione.

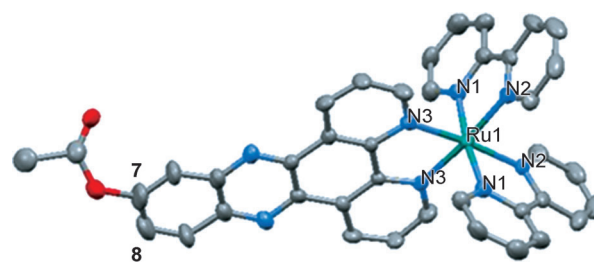


Figure 1. Crystal structure of 3. The ORTEP representation is shown at 50% probability. One disordered acetate group, hydrogen atoms and anions were omitted for clarity.

X-ray crystallography

Compound 3 crystallized as the hexafluorophosphate salt in the orthorhombic space group *Ab*a2 (Figure 1). The long axis

of the modified dppz and the ruthenium sit on the twofold rotational axis of the space group. This causes a 1:1 disorder of the position of the acetate group, which sits either on position 7 or 8.

Compound **6** crystallized with two complexes in the asymmetric unit as the mixed hexafluorophosphate/perchlorate salt in the triclinic space group $P\bar{1}$. Some water molecules are disordered, some only partially occupied. Also here, the methyl chloride substituents on position 7 are positionally disordered with ratios of 87:13 and 73:27, respectively. For the former disorder, only the chloride atom of the minor component could be localized. For the more evenly disordered methylchloride group, the whole minor moiety could be localized. Furthermore, the adjacent part of the dppz is also disordered, causing the methylchloride group to be localized closer to the long axis of the overlay of the two disordered dppz molecules (Figure S9 in the Supporting Information). In both complexes, the metal center lies in a distorted octahedral geometry. This is confirmed by the *trans*-N–Ru–N and the N–Ru–N bite angles (173.0(2)–174.0(2) and 79.0(2)–79.5(2)°, respectively, for **3** and 171.2(3)–172.1(3) and 78.3(2)–79.7(4)° for **6**); Ru–N bonds are well in accordance with reported lengths for the same kind of complexes (see Table S2 in the Supporting Information for selected angles and bond distances).^[64,65]

Photophysical properties

With complexes **1–6** in hand, the photophysical data were evaluated to obtain a better insight into their electronic properties. Data for the UV/Vis absorption of the complexes in acetonitrile and phosphate buffer solution (PBS, pH 7.01) are reported in Table 1 and Figure S10 in the Supporting Information. Assignment of absorption bands is given in the DFT calculation section and is in agreement with the literature.^[66–68]

Luminescence quantum yields (Φ_{em}) and luminescence lifetimes were evaluated to understand both the behavior of these compounds in their excited state and the influence of molecular oxygen. The Φ_{em} for all complexes were evaluated in air-equilibrated acetonitrile (Table 1) and compared with the

Φ_{em} of $[\text{Ru}(\text{bipy})_3]^{2+}$ in water ($\Phi_{em}=4.0\%$).^[69] The obtained values are comparable with the unsubstituted $[\text{Ru}(\text{bipy})_2\text{dppz}]^{2+}$ ($\Phi_{em}=2.1\%$),^[70] with the exception of **1**. This complex shows a very weak emission ($\Phi_{em}=0.1\%$), even in a hydrophobic environment, which matches what was previously reported.^[58] Luminescence lifetimes were evaluated in air-equilibrated and in degassed acetonitrile solutions (Table 1). The lifetime values for the compounds in air-equilibrated acetonitrile are in good agreement with the reported value for unsubstituted $[\text{Ru}(\text{bipy})_2\text{dppz}]^{2+}$ (180 ns).^[71] As expected, the presence of oxygen has a great influence on the lifetime of the excited state for all complexes. For complex **2**, the lifetime is almost six-times higher in the degassed solution than in the air-equilibrated one, confirming that molecular oxygen in its ground state is able to interact with the triplet excited state of the complex.

DFT calculations

In order to obtain more insights into the photophysical properties of the Ru complexes, DFT calculations were performed on complexes **1–3** and **6**. These complexes were selected since **1** and **2** showed the best biological activity (vide infra) and since we could resolve the X-ray crystal structures of **3** and **6**. Geometry optimization of the ground state and lowest-lying triplet state of complexes, together with TD-DFT singlet and triplet transition calculations were performed at the PBE0/SDD/6-31G**^[72–74] level after benchmarking the performance of several functionals and basis sets^[75] (Supporting Information). The DFT ground-state geometries (Table S3 in the Supporting Information) of **3** and **6** are in good agreement with X-ray data, although computation slightly overestimates Ru–N distances (ca. 0.03 Å for **3** and 0.035 Å for **6**). Complexes **1** and **2**, for which no X-ray structure is available, have similar ground-state structural features (Table S3). The *O* value (octahedrality value)^[76] reported in Table S3 measures the mean absolute deviation of the set of N–Ru–N angles from ideal octahedral values (that is 180° and 90°).

Complex	UV/Vis λ [nm] (ϵ [$\text{M}^{-1}\text{cm}^{-1} \times 10^{-3}$])	Emission ^[a] λ [nm] (Φ_{em})	Lifetimes [ns] ^[b]		$\log D$ ^[c]	$\Phi(^1\text{O}_2)$ at 420 nm ^[d]		
			air	degassed		PBS indirect [%]	ACN indirect [%]	ACN direct [%]
1	ACN: 287 (102.0), 317 sh (50.7), 456 (29.9) PBS: 287 (83.5), 454 (23.7)	622 (0.1)	155	390	−0.27	6	63	73
2	ACN: 287 (117.3), 397 (21.6), 450 (21.3) PBS: 286 (105.8), 401 (21.2), 442 (19.2)	623 (2.4)	184	1080	−0.42	1	69	70
3	ACN: 283 (116.5), 362 (20.3), 445 (18.6) PBS: 282 (111.6), 373 (21.1), 443 (18.4)	653 (2.7)	178	449	−0.74	2	55	65
4	ACN: 287 (107.2), 451 (22.6) PBS: 287 (94.4), 455 (23.6)	628 (1.4)	182	1000	−0.45	5	60	35
5	ACN: 284 (123.9), 370 (21.1), 451 (20.0) PBS: 284 (113.5), 374 (21.1), 445 (18.4)	630 (3.2)	194	845	−0.62	1	99	94
6	ACN: 284 (118.5), 370 (20.0), 445 (18.1) PBS: 284 (112.6), 374 (20.5), 443 (17.6)	650 (2.2)	172	534	−0.36	1	94	50

[a] Emission spectra recorded in air-equilibrated acetonitrile. [b] Lifetimes evaluated in acetonitrile. [c] Distribution coefficients between octanol and PBS (pH 7.01). [d] Average of three measurements, $\pm 10\%$.

For all complexes, DFT ground-state geometries have very close *O* values to the experimental structures. Moreover, the lowest-lying triplet state also shows *O* values that are very similar to the ground state indicating that upon formation of this state no significant geometry distortion is occurring. This finding is consistent with the emissive nature of the lowest energy triplet of **1–3** and **6** (and related compounds) in aprotic solvents as shown previously for other ruthenium polypyridyl complexes.^[76]

Eighty singlet–singlet transitions were calculated for **1–3** and **6** by TD-DFT to assign absorption bands of UV/Vis spectra. Theoretical absorptions describe well the shape of the experimental spectra, however, a blue shift of the lowest-energy bands, 325–500 nm, is observed for **1–3** and **6** (Figures S11–S14, respectively, in the Supporting Information). Calculation shows that the band centered at about 450 nm is due to two different types of MLCT transitions, one of Ru→bipy and the other of Ru→dppz character. The band in the 330–360 nm region is ligand centered ($^1\pi-\pi^*$, dppz) while the most intense band in the UV region is mixed with prevalent intraligand/ligand center nature.

The nature of the singlet–triplet transition was also investigated by TD-DFT due to the fundamental role triplet states play in the photophysical properties of ruthenium polypyridyl complexes. Notably, both DFT and UKS geometry optimization calculation (see spin density surfaces in Chart S2 in the Supporting Information) show the lowest-lying triplet state is $^3\pi-\pi^*$, although in the case of **2** a partial MLCT character is present. The excited-state diagram including singlet and triplet manifold for **1** is reported in Chart S3 in the Supporting Information (for **2**, **3** and **6** in Charts S4 and S5, respectively, in the Supporting Information). In the case of **1**, the lowest-lying triplet falls at 1.71 eV (708 nm) from the ground state, while for **2**, **3** and **6** just slightly higher, at 1.75, 1.85 (670 nm) and 1.81 eV (681 nm), respectively. At higher energy, triplets of different MLCT character are present. The obtained energy values for the lowest-lying triplet are consistent with the emission energy of the complexes in acetonitrile (although slightly underestimated) and the excited-state assignment suggests a lowest-lying state similar to the one observed for analogue dppn derivatives displaying comparable singlet oxygen conversion yields.^[50]

Singlet oxygen sensitization

From the photophysical characterization, it is clear that molecular oxygen is able to interact with the complexes in their excited state, since their emission properties are different in the presence or the absence of oxygen. Furthermore, DFT calculations on the complexes confirm that the lowest-lying state has a triplet character, which is an important requirement to allow the energy transfer from the excited PS to the molecular oxygen to bring it in the singlet state. With the photophysical characterization and the theoretical calculations in hand, a quantitative evaluation of the singlet oxygen $^1\text{O}_2(^1\Delta_g)$ production upon irradiation at 350 and 420 nm was performed in order to assess the potential of the complexes as PSs in PDT

(Table S24 in the Supporting Information for 350 nm and Table 1 for 420 nm). All compounds show a good absorbance at selected wavelength and, importantly, these wavelengths are commonly used to evaluate cytotoxic properties of potential photoactivatable anticancer agents.^[77–79]

Photosensitization of molecular oxygen was assessed using two different methods: 1) by monitoring the absorbance variations of a probe molecule, caused by a trapped $^1\text{O}_2$ adduct (indirect evaluation),^[80,81] and 2) by direct measurement of the infrared phosphorescence of $^1\text{O}_2$.^[44,50,82] The first method is based on the reaction of $^1\text{O}_2$ with an imidazole derivative to form a *trans*-annular peroxide adduct, which is able to quench the absorbance of a probe molecule, *p*-nitrosodimethyl aniline (RNO). This method can be used both in phosphate buffer solution (with histidine) and acetonitrile (with imidazole). However, we noticed that some of the complexes were already slightly quenching the absorbance of RNO upon irradiation even in the absence of imidazole. This interaction can lead, in some cases, to a unreliable quantification of $^1\text{O}_2$.^[81] Consequently, the second method, in which the presence of the $^1\text{O}_2$ is assessed directly by the detection of its phosphorescence at 1270 nm, was applied. Of note, this method can be applied in acetonitrile as well as in deuterated water, since $^1\text{O}_2$ lifetime is longer in this solvent than in H₂O. However, in our case, the amount of $^1\text{O}_2$ produced in the aqueous system was too low to give a detectable luminescence peak. The $^1\text{O}_2$ production quantum yields were evaluated for both methods by comparison with a reference molecule having a known quantum yield (phenalenone, $\Phi(^1\text{O}_2)=95\%$).^[83]

PDT photosensitizers commonly used have a $^1\text{O}_2$ quantum yield above 50%.^[84] The measured values for **1–6** in acetonitrile, for both the direct and the indirect methods, are comparable with $^1\text{O}_2$ quantum yields reported for related compounds^[39,50] and show that our complexes have a great efficacy in the photosensitization of molecular oxygen, one of the prerequisites for a PDT agent. From the values reported above, it is clear that there is an effect of the solvent on the efficiency of $^1\text{O}_2$ production. This finding is closely related to the light-switch behavior of these complexes (see also DNA binding constants evaluation section): in PBS, quenching of the excited state due to interaction of the dppz ligand with water molecules occurs very fast^[28] and does not allow the energy transfer to molecular oxygen. The quantum yields of $^1\text{O}_2$ production in PBS are therefore quite low. In acetonitrile, the photosensitization of molecular oxygen is far more efficient due to the absence of quenching mechanism on the triplet excited state. As a consequence, we anticipated that these complexes are able to produce $^1\text{O}_2$ only when they accumulate in hydrophobic compartments. This renders them more selective. Importantly, the shift of light irradiation to a higher wavelength (from 350 to 420 nm) does not affect the ability of the complexes to produce $^1\text{O}_2$. This is a favorable situation for biological applications since irradiation at 420 nm is less harmful for tissues and allow for a deeper penetration.

Distribution coefficients and human plasma stability

The cellular uptake of a molecule plays a very important role on its biological activity and is strongly influenced by the lipophilicity of the compound. Consequently, the distribution coefficients ($\log D_{\text{oct/PBS}}$) were evaluated for all complexes (Table 1). As expected, the different functional groups strongly influence the lipophilicity of the complexes, which follows the order $3 < 5 < 4 \approx 2 < 6 < 1$ (1 being the most lipophilic). Surprisingly, the most lipophilic compound, 1, contains an amino group. We assume that the lone pair of the amino group is strongly delocalized on the dppz ligand, hence avoiding protonation. Of note, all complexes are 2+ charged at physiological pH.

The stability of the complexes in human plasma was evaluated to assess the compatibility of the compounds with biological conditions. Analyses were performed following a slightly modified method that our group recently applied for other Ru^{II} complexes.^[35] The stability of the complexes was found to be different based on the functional group that they bear. Compounds 1, 2 and 5 displayed a very good stability in human plasma over 48 h of incubation, as clearly shown on the LC-MS chromatograms presented in Figure S15 in the Supporting Information (see also Table S25 in the Supporting Information). Compound 3 turned out to be not stable in human plasma since incubation at 37 °C led to its decomposition already at $t=0$, when most of the compound has already been transformed into 4 due to the hydrolysis of the acetyl moiety. Complex 4 showed partial lability and after 4 h incubation the comparison with diazepam (internal standard) indicated that one third of the complex was still intact. Complex 6 was also not stable in human plasma at 37 °C. This is clear from the LC-MS chromatogram (Figure S15 in the Supporting Information), where a peak at $t=0$ corresponding to the hydrolysis of the chloride to a hydroxyl group (compound 5), is already present. After 48 h of incubation, the peak of 6 was no longer present and only the hydroxyl derivative was detectable. It is worth noting that the LC-MS analyses showed that 1, 2, 4 and 5 were stable in water at 37 °C when monitored over a period of 48 h, while 3 and 6 already showed partial hydrolysis to 4 and 5, respectively, over 48 h incubation in water.

DNA-binding constant evaluation

Ru polypyridyl complexes are well known to interact with double-stranded DNA in a noncovalent manner by intercalation or groove binding.^[71,85,86] This very close interaction between the compounds and DNA can be favorable for PDT applications. It is indeed extremely important that the PS localizes in very close proximity to the target system since ¹O₂ is a very reactive species, the half-life of which in a biological environment is estimated to about 40 ns, which corresponds to a range of action of around 20 nm.^[5] Intercalation of the complex in the DNA double helix will enable ¹O₂ generation to happen very close to DNA and hence allow an efficient oxidation of the genetic material. Consequently, the binding affinity of all complexes for double-stranded DNA was evaluated. For such complexes, interaction with DNA also produces the so-

called light-switch effect,^[28,62] which is exploited to image these compounds in living cells.^[87] Specifically, when the complex is intercalated into the DNA helix, the ligand is situated in a hydrophobic pocket shielded from water molecules and the nonradiative quenching of the excited state, which happens in aqueous environment, is not possible. As a consequence, the energy of the excited state is released by phosphorescence.^[28] Quantitative evaluation of the affinity of the six Ru complexes for double-stranded DNA was therefore carried out by spectroscopic studies. Titration was performed using calf thymus (CT) DNA for all complexes and changes in the emission spectra were monitored.^[62,66] The spectroscopic data collected were fitted using the Bard equation^[66,86,88] to obtain the binding constants (K_b) and the sizes of the site of interaction (s). These values are reported in Table 2. Figure S16 in the Supporting Information shows emission curves for the complexes during the titrations. The initial luminescence is negligible in PBS in the absence of CT-DNA. Upon CT-DNA concentration increase, the luminescence is strongly enhanced until saturation is reached. In the absorbance spectrum of 2 (Figure S17 in the Supporting Information) recorded before the addition of DNA to the sample and once the DNA saturation was reached, the peak at 400 nm decreases in intensity due to the stacking of the chromophore between the DNA nucleobases. This evidence confirms that this complex has an intercalative mode of interaction with CT-DNA.^[62] Of note, the maximum shifts to 425 nm during the titration. All other complexes studied in this work showed a similar behavior (Figure S16). The K_b values obtained are comparable to the known intercalator [Ru(bipy)₂dppz]²⁺ ($> 10^6$).^[66] It can be concluded that the presence of a substituent on the dppz system is not significantly affecting the ability of the complexes to strongly interact with DNA.

Table 2. DNA-binding constants (K_b) and binding site sizes (s).

Complex ([μM])	K_b [M ⁻¹ per nucl] × 10 ⁶	s [bp]
1 (9)	1.5 ± 0.5	3.8 ± 0.3
2 (0.6)	21.5 ± 3.8	4.0 ± 0.2
3 (5)	8.2 ± 1.8	2.2 ± 0.1
4 (5)	3.4 ± 0.8	2.6 ± 0.1
5 (1)	13.9 ± 3.7	2.8 ± 0.2
6 (1)	9.1 ± 2.2	2.5 ± 0.2

Dark cytotoxicity and phototoxicity

Having established that all Ru compounds produce a high level of ¹O₂ in hydrophobic environments, their toxicity on cervical cancer (HeLa) and non-cancerous (MRC-5) cell lines was investigated. All complexes were found to be noncytotoxic in the dark ($IC_{50} > 100 \mu\text{M}$) when incubated for 48 h with both cell lines (Table 3). The effect of light irradiation in enhancing the cytotoxicity was evaluated by incubating HeLa cells for 4 h with the metal complexes and exposing them to two different light treatments: 10 min at 350 nm (2.58 J cm⁻²) and 20 min at 420 nm (9.27 J cm⁻²). As a control, untreated cells were also exposed to the same irradiation procedure and, as expected, the

light alone was found to be nontoxic. It is worth noting that the light doses employed in this work are well comparable or even lower to those employed for activation of other Ru-containing photosensitizers^[39] ($2\text{--}11.5\text{ J cm}^{-2}$ at $500\text{--}600\text{ nm}$) or metal-based phototoxic compounds^[77] (5 J cm^{-2} at 350 nm). For comparison purposes, Photofrin reaches a phototoxicity of $4.3\text{ }\mu\text{M}$ when irradiated with a light dose of 5 J cm^{-2} .^[56,89] Upon light irradiation, our compounds showed a different cytotoxic profile, following the order $3 \approx 5 < 4 < 6 < 2 < 1$. Complexes **3** and **5** were found to be nonphototoxic both at 350 and 420 nm . Complexes **4** and **6** showed no or just weak activity ($47.5\text{ }\mu\text{M}$) when irradiated at 350 nm . However, irradiation at 420 nm induced a moderate activity for both compounds, with an increase in the cytotoxicity of more than five times. Of great interest, **1** and **2** showed remarkable phototoxic effect, especially when irradiated at 420 nm , with IC_{50} values of 2.0 and $5.5\text{ }\mu\text{M}$, respectively. Of outmost interest, these values are well comparable with the activity of Photofrin and cisplatin, which are approved PDT and chemotherapeutic agents, respectively.^[56,89] Importantly, both compounds showed a stronger phototoxic effect at the higher wavelength (420 nm), where light is less harmful for tissues. However, phototoxicity in itself is not the only requirement in the development of a PDT agent. A successful PS must be characterized by a high PI. Consequently, it was of high interest to determine the maximum dark toxicity on HeLa cells for the two most active compounds. Impressively, **2** was found to be nontoxic up to a concentration of $235\text{ }\mu\text{M}$. Hence, the toxicity of **2** is increased 42-fold upon irradiation of the cells at 420 nm . Complex **1** showed an even lower dark toxicity: the compound presented an IC_{50} higher than $300\text{ }\mu\text{M}$, which is the maximum concentration reachable in cell culture medium before precipitation. In this case, the activity of the compound is improved by more than 150-times upon light activation. These values are indeed really promising considering that the frequently used PS available on the market (Photofrin and hypericin)^[7] have a PI of >10 and >43 , respectively.^[89] Due to the very promising activity of **1** and **2**, their possible phototoxicity towards the MRC-5 cell line was also investigated (Table S26 in the Supporting Information). As expected, the phototoxicity of **1** and **2** followed the same trend observed for HeLa cells. The only difference is that **1** does not display any phototoxic activity upon irradiation at 350 nm . This observation can be due to the fact that **1** has a singlet oxygen quantum yield two-times lower upon irradiation at 350 nm than at 420 nm .

Cellular uptake

A crucial parameter for the biological activity of a molecule is the cellular uptake, which is strongly influenced by the structure of the molecule itself. Consequently, it was of interest to investigate the possible correlation between structural modifications, antiproliferative effect and cellular penetration of the target compounds. To have a definitive assessment of the uptake of these complexes inside the cell, we can take advantage from the presence of a metal in our systems. The presence of the ruthenium allows the use of a number of different ana-

Table 3. IC_{50} values for all the complexes incubated with MRC-5 and HeLa cells in the dark and upon light irradiation.

$\text{IC}_{50}\text{ }\mu\text{M}$	MRC-5 dark ^[a]	HeLa dark ^[a]	HeLa 350 nm ^[b]	HeLa 420 nm ^[c]	PI 420 nm
1	>100	>300	25.1 ± 7.6	2.0 ± 0.9	>150
2	>100	235.5 ± 24.7	9.0 ± 1.4	5.5 ± 0.7	42
3	>100	>100	>100	>100	n.d. ^[d]
4	>100	>100	>100	20.8 ± 1.0	>5
5	>100	>100	>100	>100	n.d. ^[d]
6	>100	>100	47.5 ± 9.4	20.5 ± 4.4	>5
cisplatin	16.8 ± 1.8	8.9 ± 2.6	26.8 ± 1.7	26.8 ± 2.4	-

[a] 48 h incubation; [b] 4 h incubation, light dose 2.58 J cm^{-2} ; [c] 4 h incubation, light dose 9.27 J cm^{-2} ; [d] not determinable.

lytical techniques that are not applicable for metal-free organic molecules. Hence, we performed HR-CS AAS, a technique that enables accurate measurements of metal traces in biological samples and that has already been applied for ruthenium complexes in previous studies.^[35,90] For this purpose, HeLa cells were incubated with the compounds at $20\text{ }\mu\text{M}$ concentration for 4 h in the dark. Ruthenium uptake into whole cells was quantified by HR-CS AAS while their cellular protein content was evaluated using the Bradford method.^[91] These two values were correlated to obtain the nmol of ruthenium per mg of proteins in cells, as reported in Figure 2. Remarkably, the uptake profile correlates really well with the anticancer activity of the target complexes, as the more toxic compounds turned out to have the higher cellular accumulation. The complexes indeed showed the following order of uptake: $3 < 5 \approx 4 \approx 6 < 1 < 2$, proving the importance of the chemical modification on the dppz ligand. The very good cellular uptake for complexes **1** and **2** (1.08 and $1.76\text{ nmol Ru per mg protein}$, for **1** and **2**, respectively) is also well comparable with that of recently published ruthenium anticancer drug candidates.^[33] As a further characterization of the biological behavior of the two most cell penetrating complexes (**1** and **2**), AAS studies were performed to evaluate their uptake on MRC-5 cells. Interestingly, the uptake of **1** and **2** on MRC-5 cells presented a reversed situation for the two compounds (Table S26 in the Supporting Information). The uptake of **1** ($0.76\text{ nmol Ru per mg protein}$) was almost comparable with the one in HeLa cells, while **2** ($0.18\text{ nmol Ru per mg protein}$) penetrated about 10-times less in MRC-5 than in HeLa cells. Despite this difference in cellular accumulation, the antiproliferative activity of **2** on MRC-5 was comparable to that on HeLa cells.

Cellular localization

Since complexes **1** and **2** demonstrated a remarkable stability, interesting uptake and valuable phototoxicity, we decided to investigate their biological profile in more detail. To have a deeper insight on the cellular biodistribution of the compounds, we exploited the known luminescence characteristic of polypyridyl Ru^{II} complexes to visualize them in HeLa cells by confocal microscopy.^[87] For **1**, only a very weak luminescence in the whole cell could be detected even when the cells were

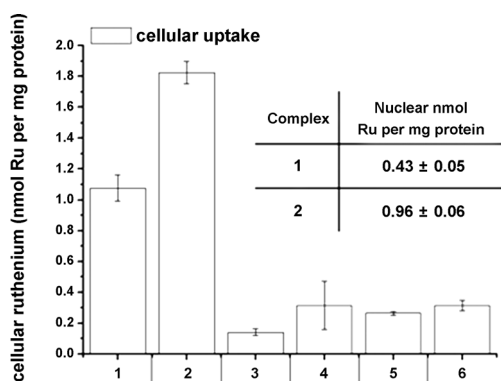


Figure 2. Cellular uptake into HeLa cells treated for 4 h with 20 μM solution of the target ruthenium complexes. Results are expressed as the mean \pm standard deviation of independent experiments. Inset: nuclear uptake for complexes 1 and 2.

incubated with 100 μM of the complex (see Figure S18 in the Supporting Information, top). As reported in Table 1, **1** has a significantly lower luminescence quantum yield than the other complexes, even in hydrophobic media. This could explain the difficulties in detecting its presence in cells by confocal microscopy. We recently reported that luminescent Re-Mn-containing peptide nucleic acid (PNA) bioconjugates could not be detected by fluorescence microscopy although their presence in cells could be confirmed by HR-CS AAS.^[92] On the contrary, microscopy studies revealed a main target for **2**, which is able to penetrate the cellular membrane after just 2 h of incubation and to accumulate preferentially in the nucleus, as shown in Figure 3 and Figure S18 (bottom). This accumulation is not surprising since Ru^{II} polypyridyl complexes are well known to target the nucleus and this feature is already exploited for imaging.^[29]

However, fluorescence microscopy might not be completely exhaustive to assert the whole localization of such complexes

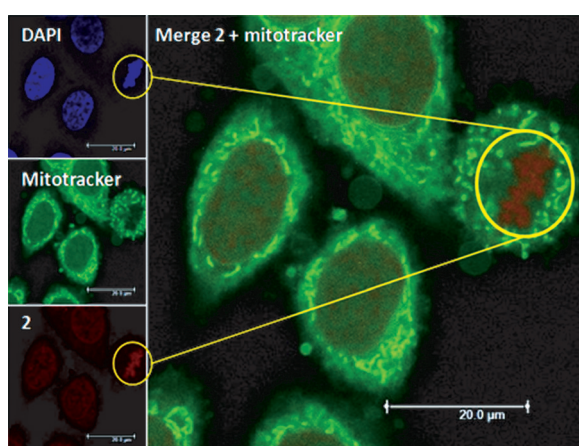


Figure 3. Cellular localization of complex **2**. Confocal microscopy localization experiments on HeLa cells treated for 2 h with 100 μM of complex **2** (excitation at 488 nm, emission above 600 nm, bottom left) and stained with DAPI (nuclear staining, top left) and with Mitotracker green (mitochondrial staining middle left); the yellow circle shows a representative example of the different localization of **2** and Mitotracker green (picture on the right).

due to the quenching effect in aqueous environment. Further experiments were therefore conducted by HR-CS AAS to determine the specific nuclear accumulation of **2**. Moreover, complex **1** was included in the study since it displayed a phototoxic behavior similar to **2**. This analysis allows overcoming its low luminescence quantum yield, which is a limit to the evaluation of its localization by luminescence microscopy. As reported in Figure 2 (inset), **1** and **2** indeed displayed strong accumulation in the nucleus with 0.43 and 0.96 nmol Ru per mg protein, respectively. Even though the data come from two different sets of experiments and are not directly comparable, the results obtained follow the same trend observed for the uptake in the whole cell, with cells incubated with complex **2** showing roughly twice the amount of ruthenium than in case of incubation with compound **1**.

Given the preferential accumulation of complexes **1** and **2** in the nuclear compartment and the strong DNA binding affinity (see DNA-binding constants evaluation section), it is reasonable to hypothesize that the compounds could exert their mode of action at a nuclear level. These findings, together with their impressive phototoxic index, strongly suggested a specific light-mediated mechanism of phototoxicity that affects the DNA.

DNA photocleavage

Coherently with the previous assumptions, we decided to investigate the effect of **1** and **2** on plasmid DNA upon light irradiation. The production of ROS, and in particular singlet oxygen, is known to generate oxidative damage to nucleic acids.^[5] The ability of metal complexes to produce ROS is already known to play an important role in the photoactivatable cleavage of DNA.^[93,94] For a circular plasmid DNA, the intact supercoiled form is a fast migrating band (Form I). When one of the strands is subjected to cleavage (nicking), a circular but open form is generated, which migrates slower in the gel (Form II). A linear species (Form III), which appears between the other two, is formed when both strands undergo cleavage.^[95] As previously performed by our group on rhenium complexes,^[78] supercoiled pcDNA3 plasmid was treated with increasing concentrations of the compounds (1–50 μM) and irradiated at 420 nm for 20 min (9.27 J cm⁻²). A negative control with the plasmid treated with **1** and **2** (50 μM) in the dark was used for comparative purposes. A positive control with the plasmid treated with a restriction enzyme, namely BstXI, was performed to visualize the linearized band (Figure S19 in the Supporting Information). As can be noticed in Figure 4, the complexes are able to efficiently photocleave plasmid DNA. They showed a strong effect already at a concentration of 10 μM after irradiation at 420 nm, decreasing substantially the amount of Form I and allowing the appearance of Form II. For higher concentrations, Form I disappeared while the intensity of the nicked band increased and the linear form was also visible. Interestingly, DNA treated in the dark with the compounds (50 μM , lanes 7) did not show any significant alterations. Notably, complex **1** showed already a slight effect at a concentration of 1 μM ; these data are in good agreement with its stronger

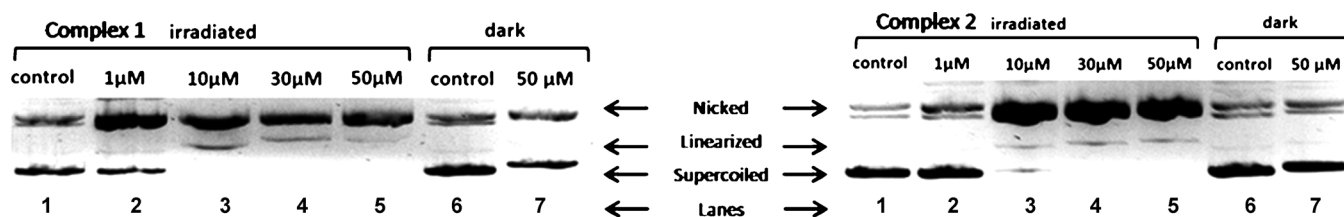


Figure 4. Gel electrophoresis of plasmid DNA photocleavage experiments with complexes **1** and **2** upon irradiation at 420 nm. pcDNA3 plasmid untreated and irradiated for 20 min at 420 nm (lanes 1); plasmid treated with **1** (left) and **2** (right) at different concentrations and irradiated (lanes 2–5); plasmid untreated in the dark (lanes 6); plasmid treated with **1** (left) and **2** (right) at 50 μM in the dark (lanes 7). The results were repeated and one experiment is depicted.

phototoxicity (2 μM), compared with **2**. Moreover, the effective concentrations in this experiment are close to the respective IC_{50} values upon irradiation at 420 nm.

Conclusions

While ruthenium complexes are well known for their biological activity against cancer cells, the application of substitutionally inert polypyridyl Ru complexes as PDT agents has only been scarcely studied despite their appealing photophysical properties. In this work, we clearly demonstrate the potential of this class of compound as PS by reporting a detailed photophysical and biological evaluation of six $[\text{Ru}(\text{bipy})_2\text{dppz}]^{2+}$ derivatives.

As expected for PDT agents, all complexes showed moderate to very good ability to produce $^1\text{O}_2$. The $^1\text{O}_2$ quantum yields obtained were found to be dependent on the lipophilicity of the medium used during the experiments. This characteristic is connected to the light-switch property of DNA-intercalating complexes containing the dppz ligand. This can confer a further selectivity to the compounds since the production of the toxic species will occur only when the complexes are accumulating in hydrophobic cellular compartments. DFT calculations performed on four of the compounds (**1**, **2**, **3** and **6**) highlight the triplet character of the excited state, confirming the possibility of the interaction between the excited state of the complexes and the ground state of molecular oxygen. As expected, the complexes show a strong interaction with double stranded DNA due to the presence of the dppz intercalating ligand. $^1\text{O}_2$ can be produced in the very proximity of DNA, the oxidation target. Importantly, all compounds are nontoxic in the dark on the two cell lines studied in this work, whereas, upon light irradiation, **1** and **2** show a remarkable phototoxicity on HeLa cells, comparable with Photofrin.^[56,89] In particular, the phototoxic index of **2** is 42 when irradiated at 420 nm. Impressively, this index is even higher in case of complex **1**, reaching a value of more than 150 at 420 nm. This wavelength is very interesting for biological applications because of the higher penetration ability and lower toxicity for tissues. At the same time, irradiation at 420 nm allows for a more localized therapy, since the light will not diffuse to the healthy tissues in a non-controllable manner. Moreover, the intensity of the irradiated light used during the course of our experiments (2.58 J cm^{-2} at 350 nm and 9.27 J cm^{-2} at 420 nm) is well comparable to (or even lower than) the one used for related compounds^[39] and guarantees the absence of damage to untreated cells.^[96] Cellu-

lar localization and uptake on HeLa cells were studied by luminescence microscopy and HR-CS AAS. While for complexes **3–6** a minimal cellular penetration was determined, AAS analysis showed that **1** and, to a major extent, **2** had a very good cellular uptake, comparable to other Ru complexes studied with these techniques.^[33] Moreover, preferential nuclear accumulation was confirmed for both compounds. This gives an indication for a possible mode of action operating at the nuclear level. This assumption is supported by the strong affinity for DNA of the Ru^{II} complexes. Interestingly, DNA photocleavage experiments confirmed our hypothesis and highlight the high importance of the light-mediated DNA damage for the overall phototoxicity. In particular, the conversion of the supercoiled (intact) form to the nicked (damaged) form occurs in a dose-dependent manner, with effective concentrations lying in the same range of the IC_{50} values obtained from the antiproliferative experiments. In conclusion, complexes **1** and **2** show a great potential as novel and innovative metal-based PDT agents due to their preferential nuclear accumulation, extremely competitive phototoxic index and very efficient light-induced DNA cleavage.

Experimental Section

Materials

All chemicals were of reagent-grade quality or higher, were obtained from commercial suppliers and were used without further purification. Solvents were used as received or dried over molecular sieves.

Instrumentation and methods

^1H and ^{13}C NMR spectra were recorded in deuterated solvents on a Bruker DRX 400 (^1H : 400 MHz, ^{13}C : 100.6 MHz) or 500 (^1H : 500 MHz, ^{13}C : 126 MHz) MHz spectrometers at room temperature. The chemical shifts, δ , are reported in ppm (parts per million). Residual solvent peaks were used as an internal reference. The abbreviations for the peak multiplicities are as follows: s (singlet), d (doublet), dd (doublet of doublets), t (triplet), q (quartet), m (multiplet), and br (broad). ESI mass spectra were recorded on a Bruker Esquire 6000 spectrometer. Elemental microanalyses were performed on a LecoCHNS-932 elemental analyzer. IR spectra were obtained with a PerkinElmer FTS PRO spectrometer.

Synthesis

[Ru(bipy)₂-dppz-7-amino][PF₆]₂ (1)

1 was synthesized as previously reported.^[58,59] Experimental data fit with the literature. Purity of **1** was assessed by elemental analysis. Elemental analysis calcd for C₃₈H₃₃F₁₂N₉O₃P₂Ru (%): C 43.27, H 3.15, N 11.95; found: C 43.44, H 3.11, N 11.95.

[Ru(bipy)₂-dppz-7-methoxy][PF₆]₂ (2)^[60]

The complex was prepared by adapting a literature reported procedure (yield: 282 mg, 72%), since the hexafluorophosphate salt of [Ru(bipy)₂phenidione]²⁺ was used as precursor and **2** was isolated as PF₆⁻ salt.^[60] The spectroscopic data match well with those reported for the complex with a ClO₄⁻ counter anion. The purity of **2** was checked by elemental analysis. Elemental analysis calcd for C₃₉H₂₈F₁₂N₈O₂P₂Ru: C 46.12, H 2.78, N 11.03; found: C 46.03, H 2.75, N 10.96.

4-Hydroxy-phenylenediamine dicarbamate

THF (10 mL) was added to a mixture of 4-hydroxy-phenylenediamine (100 mg, 0.81 mmol) and di-*tert*-butyl dicarbonate (385 mg, 1.77 mmol). The mixture was stirred for 24 h at room temperature under N₂ atmosphere. THF was then evaporated and the residue was dissolved in EtOAc (50 mL). The organic phase was then washed with 0.5 M HCl (until the aqueous layer became colorless), distilled water (1 × 50 mL) and brine (1 × 50 mL). The organic phase was then dried over anhydrous MgSO₄, filtered and concentrated. Flash column chromatography (silica gel, hexane/EtOAc 3:1 → 2:1) gave the product as a white solid (yield: 112 mg, 43%). ¹H NMR (400 MHz, [D₆]acetone): δ = 1.49 (s, 9H), 1.51 (s, 9H), 6.58 (m, 1H), 7.15 (d, 1H), 7.29 (s, 1H), 7.70 (s, br, 1H), 7.77 (s, br, 1H), 8.26 ppm (s, 1H); ¹³C NMR (100.6 MHz, [D₆]acetone): δ = 27.5, 27.6, 79.1, 79.3, 109.1, 110.5, 121.1, 126.5, 133.6, 153.0, 154.3, 155.1 ppm; ESI-MS (pos. detection mode): *m/z* (%): 347.1 (100) [M + Na]⁺.

4-Acetoxy-phenylenediamine dicarbamate (7)

NEt₃ (311 mg, 3.08 mmol) and acetyl chloride (0.2 mL, 3.08 mmol) were added to a stirred solution of 4-hydroxy-phenylenediamine dicarbamate (200 mg, 0.62 mmol) in CH₂Cl₂ (25 mL). After being stirred at room temperature for 1.5 h, the reaction mixture was diluted with CH₂Cl₂ (100 mL). The organic phase was washed with sat. NaHCO₃ (1 × 100 mL), distilled water (1 × 100 mL) and brine (1 × 50 mL). The organic phase was then dried over anhydrous MgSO₄, filtered and concentrated. Flash column chromatography (silica gel, hexane/EtOAc 3:1 → 2:1) gave **7** as a white sticky solid (yield: 205 mg, 91%). ¹H NMR (500 MHz, CDCl₃): δ = 1.40 (s, 18H), 2.15 (s, 3H), 6.37 (s, br, 1H), 6.72–6.78 (m, 2H), 7.26 (s, 1H), 7.39 ppm (s, br, 1H); ¹³C NMR (126 MHz, CDCl₃): δ = 21.1, 28.3, 28.4, 81.1, 81.2, 116.1, 116.2, 117.5, 125.7, 129.1, 148.4, 153.1, 153.7, 169.3 ppm; ESI-MS (pos. detection mode): *m/z* (%): 389.1(100) [M + Na]⁺.

[Ru(bipy)₂-dppz-7-acetoxy][PF₆]₂ (3)

TFA (4 mL) was added slowly at 0 °C to a stirred solution of **7** (180 mg, 0.49 mmol) in CH₂Cl₂ (10 mL). After 20 min, the ice bath was removed and the mixture was stirred at room temperature for 2 h. The solvent and TFA were then evaporated using a high vacuum pump. The residue was diluted with CH₂Cl₂ (100 mL) and washed with a sat. NaHCO₃ solution (1 × 200 mL). The organic phase was separated and the aqueous phase was back-extracted with CH₂Cl₂ (50 mL). The combined organic layers were dried over

anhydrous MgSO₄, filtered and concentrated to give 3,4-diaminophenyl acetate (50 mg, 61%) that was used directly for the next step.

A stirred solution of 3,4-diaminophenyl acetate (40 mg, 0.24 mmol) and [Ru(bipy)₂phenidone](PF₆)₂ (146 mg, 0.16 mmol) in 16 mL of 1:3 CH₃CN/EtOH (v/v) was heated at 75 °C under N₂ atmosphere. After 2.5 h, the mixture was concentrated using a rotary evaporator and cooled to room temperature. Addition of a sat. NH₄PF₆ (10 mL) solution resulted in the formation of an orange precipitate. The precipitate was filtered, washed with distilled water, ice cold ethanol and finally with diethyl ether to give **3** as a red-orange powder (yield: 109 mg, 65%). ¹H NMR (500 MHz, [D₆]DMSO): δ = 2.45 (s, 3H), 7.40 (t, 2H), 7.61 (t, 2H), 7.76 (d, 2H), 7.84 (d, 2H), 8.02–8.07 (m, 3H), 8.15 (t, 2H), 8.22–8.26 (m, 4H), 8.30 (d, 1H), 8.57 (d, 1H), 8.89 (dd, 4H), 9.62 (d, 1H), 9.64 ppm (d, 1H); ¹³C NMR (126 MHz, [D₆]DMSO): δ = 21.6, 120.3, 124.8, 124.9, 128.1, 128.3, 129.2, 130.4, 130.5, 131.1, 133.6, 133.7, 138.4, 138.5, 140.3, 140.5, 140.9, 142.7, 150.7, 150.8, 151.8, 152.3, 153.3, 153.8, 154.0, 156.9, 157.2, 169.5 ppm; ESI-MS (pos. detection mode): *m/z* (%): 376.9 (100) [M – 2PF₆]²⁺. Elemental analysis calcd for C₄₀H₂₈F₁₂N₈O₂P₂Ru: C 46.03, H 2.70, N 10.74; found: C 45.90, H 2.68, N 10.79.

[Ru(bipy)₂-dppz-7-hydroxy][PF₆]₂ (4)

To a stirred solution of **3** (50 mg, 0.048 mmol) in MeOH (6 mL), 1 M aq. NaOH (4 mL) was added. After being stirred at room temperature for 1.5 h, the reaction mixture was concentrated and acidified with 1 M HCl until pH of about 2. The color of the solution changed from deep red to light orange upon acidification. Solid NH₄PF₆ was then added until the precipitation was complete. The orange precipitate was then filtered, washed with distilled water (10 mL), ice-cold ethanol (10 mL) and finally with diethyl ether (15 mL) to give **4** as an orange powder (yield: 45 mg, 94%). ¹H NMR (500 MHz, [D₆]DMSO): δ = 7.38 (t, 2H), 7.59–7.62 (m, 3H), 7.75–7.78 (m, 3H), 7.84 (d, 2H), 7.98–8.01 (m, 2H), 8.12–8.24 (m, 6H), 8.37 (d, 1H), 8.87 (dd, 4H), 9.55 (d, 1H), 9.62 (d, 1H), 11.34 ppm (s, br, 1H); ¹³C NMR (126 MHz, [D₆]DMSO): δ = 108.5, 124.8, 124.9, 127.2, 127.9, 128, 128.2, 128.3, 130.5, 130.8, 131.4, 133.1, 133.5, 137.3, 138.3, 138.4, 140.3, 144.6, 149.7, 150.8, 151.8, 152.3, 153.1, 153.6, 156.9, 157.2, 161.6 ppm; ESI-MS (pos. detection mode): *m/z* (%): 356 (100) [M – 2PF₆]²⁺. Elemental analysis calcd for C₃₈H₂₆F₁₂N₈O₂P₂Ru·H₂O: C 44.76, H 2.77, N 10.99; found: C 44.87, H 2.79, N 10.93.

3,4-Diaminobenzoic acid ethyl ester

Concentrated sulfuric acid (12 mL) was added dropwise to a solution of 3,4-diaminobenzoic acid (1.30 g, 8.54 mmol) in EtOH (100 mL). The mixture was then refluxed for 6 h. The solution was neutralized by the addition of sat. NaHCO₃ (300 mL). The neutral aqueous solution was extracted with EtOAc (200 mL). The reunited organic phases were dried over anhydrous MgSO₄, filtered and the solvent was evaporated to afford the product as a brown powder (yield: 1.37 g, 89%). ¹H NMR (300 MHz, CDCl₃): δ = 1.33–1.38 (t, 3H), 4.27–4.34 (q, 2H), 6.65–6.68 (d, 1H), 7.41 (d, 1H), 7.45–7.49 ppm (dd, 1H); ESI-MS (pos. detection mode) *m/z*: 203.0 [M + Na]⁺, 383.1 [2M + Na]⁺.

1,2-Diaminobenzyl alcohol (8)

LiAlH₄ (442 mg, 11.65 mmol) was added in portions over 10 min to a stirring solution of 3,4-diaminobenzoic acid ethyl ester (700 mg, 3.88 mmol) in dry THF (35 mL) cooled at 0 °C. The mixture, which turned from brown to greenish, was stirred at 60 °C for 45 min

under inert conditions. The mixture was then cooled to 0 °C and water (2 mL) was carefully added. The mixture, which turned brown, was stirred for 1 h. The suspension was then filtrated to remove undissolved residue, which was thoroughly washed with THF. The brown filtrate was dried under vacuum. The desired product was isolated by flash column chromatography on silica gel with ether/methanol (10:1) as the eluent to first separate the by-product 1,2-diaminotoluene, then with ether/methanol (10:3) to collect **8** (yield: 180 mg; 33%). ¹H NMR (300 MHz, CDCl₃): δ = 4.52 (s, 2H), 6.68–6.73 ppm (m, 3H); ESI-MS (pos. detection mode): *m/z* (%): 160.9 (100) [M+Na]⁺.

[Ru(bipy)₂-dppz-7-hydroxymethyl][PF₆]₂ (**5**)

To a stirring solution of [Ru(bipy)₂phenidone](PF₆)₂ (720 mg, 0.79 mmol) in CH₃CN (15 mL) and one drop of acetic acid, **8** (120 mg, 0.87 mmol) in CH₃CN (5 mL) was added dropwise. The mixture, which turned from dark brown to deep red, was refluxed for 1 h. The solution was then concentrated to 5 mL and a sat. aqueous solution of NH₄PF₆ (50 mL) was added. The product, which precipitated as a PF₆ salt, was isolated by filtration, then washed with water and purified by flash column chromatography on silica gel with CH₃CN/KNO₃ aqueous solution 0.4 M (10:1) as the eluent. The fractions containing the product were reunited and the eluent was dried on a rotary evaporator. Workup of the reunited fractions after the column: CH₃CN (30 mL) was added to the residue and undissolved KNO₃ was removed by filtration. The red filtrate was dried again and redissolved in water (40 mL). NH₄PF₆ was then added to make the complex precipitate as a PF₆ salt, which was collected by filtration, washed with water (20 mL) and diethyl ether (25 mL) and dried on a vacuum pump, to obtain **5** as a red powder (yield: 390 mg, 48%). A pure sample for elemental analysis was obtained by further purification with flash column chromatography on silica gel with CH₃CN/KNO₃ aqueous solution 1.3 M/H₂O (100:15:15) as the eluent. Purity of the fractions was assessed by RP HPLC (*t* = 0–3 min 95% H₂O 0.1% TFA, 5% CH₃CN; *t* = 17 min 100% CH₃CN; *t* = 22 min 100% CH₃CN). After the column, the same workup was performed to obtain the complex as a PF₆ salt. ¹H NMR (400 MHz, CD₃CN): δ = 4.96 (s, 2H), 7.25–7.28 (m, 2H), 7.47–7.48 (t, 2H), 7.73–7.75 (t, 2H), 7.85–7.89 (m, 4H), 8.00–8.06 (m, 3H), 8.10–8.13 (t, 2H), 8.16–8.17 (m, 2H), 8.33 (s, 1H), 8.38–8.39 (d, 1H), 8.51–8.56 (dd, 4H), 9.60–9.62 ppm (dd, 2H); ¹³C NMR (126 MHz, CD₃CN): δ = 64.11, 125.30, 125.36, 126.27, 128.37, 128.38, 128.51, 128.64, 130.37, 131.88, 131.91, 132.63, 134.39, 134.526, 138.919, 139.00, 140.57, 140.99, 143.21, 143.90 ppm; ESI-MS (pos. detection mode): *m/z* [M–2PF₆]²⁺ 363.2, [M–PF₆]⁺ 871.0. Elemental analysis calcd for C₃₉H₂₈F₁₂N₈OP₂Ru (%): C 46.11, H 2.77, N 11.03; found: C 45.93, H 2.80, N 10.89.

[Ru(bipy)₂-dppz-7-chloromethyl][PF₆]₂ (**6**)

DMF (175 μL, 2.26 mmol) was added dropwise to a stirring solution of (COCl)₂ (194 μL, 2.26 mmol) in CH₃CN (5 mL) cooled at 0 °C. The mixture was slowly warmed to room temperature and stirred for 15 min. It was then cooled to 0 °C and a solution of **5** (230 mg, 0.226 mmol) in CH₃CN (5 mL) was added dropwise to the mixture, which was then stirred at room temperature, overnight. The solution was then concentrated to 5 mL and a sat. aq. solution of NH₄PF₆ (40 mL) was added. The red precipitate was collected by filtration, washed with water (20 mL) and diethyl ether (25 mL), and dried using a high vacuum pump. A sample for elemental analysis was obtained by further purification with flash column chromatography on silica gel with CH₃CN/KNO₃ aqueous solution 1.3 M/H₂O (100:15:15) as the eluent. The purity of the fractions was assessed

by RP HPLC (see synthesis of **5**). After the column, the same workup as complex **5** was performed to obtain the complex as the PF₆ salt. ¹H NMR (400 MHz, CD₃CN): δ = 5.04 (s, 2H), 7.25–7.29 (t, 2H), 7.45–7.49 (m, 2H), 7.73–7.76 (d, 2H), 7.85–7.90 (m, 4H), 8.00–8.04 (t, 2H), 8.10–8.18 (m, 5H), 8.44–8.46 (m, 2H), 8.51–8.57 (dd, 4H), 9.61–9.64 ppm (d, 2H); ¹³C NMR (126 MHz, CD₃CN): 46.38, 125.31, 125.37, 128.48, 128.51, 128.66, 131.21, 131.76, 131.79, 133.96, 134.54, 134.59, 138.94, 139.03, 141.35, 141.45, 143.42, 143.45, 143.54, 151.52, 151.54, 153.17, 153.19, 154.82, 154.84, 158.23, 158.23 ppm; ESI-MS (pos. detection mode): *m/z* [M–2PF₆]²⁺ 372.1, [M–PF₆]⁺ 888.9. Elemental analysis calcd for C₃₉H₂₇ClF₁₂N₈P₂Ru (%): C 45.29, H 2.63, N 10.83; found: C 44.95, H 2.64, N 10.55.

Spectroscopic studies

UV/Vis measurements were performed on a Varian Cary 50-Scan UV/Vis spectrophotometer. For luminescence quantum yield measurements, emission spectra were recorded with a Varian Cary Eclipse fluorescence spectrophotometer equipped with a Hamamatsu R3896 photomultiplier tube as detector, where the sample temperature can be controlled by a Peltier thermostatic system. Emission spectra were corrected for the spectral sensitivity of the detection system by standard correction curves. The emission intensities were normalized to a nominal absorption value of 0.1. Quantum yields in aerated acetonitrile were determined by comparison with the emission of [Ru(bipy)₃]Cl₂ in aerated water (Φ = 0.040).^[69] Luminescence lifetime measurements were recorded on an Edinburgh LP920 laser flash photolysis transient absorption spectrometer using a flashlamp pumped Q-switched Nd:Yag laser (355 nm) as excitation source.

X-ray crystallography

Crystallographic data of compound **3** were collected at 183(2) K with MoK_α radiation (λ = 0.7107 Å) that was graphite-monochromated on a Stoe IPDS2 diffractometer and of compound **6** on an Agilent SuperNova, Dual source, with an Atlas detector and CuK_α radiation (λ = 1.54184 Å). Suitable crystals were covered with oil (Infinitec V8512, formerly known as Paratone N), placed on a nylon loop that is mounted in a CrystalCap Magnetic™ (Hampton Research) and immediately transferred to the diffractometer. In the case of the IPDS2, a maximum of eight thousand reflections distributed over the whole limiting sphere were selected by the program SELECT and used for unit cell parameter refinement with the program CELL.^[97] Data were corrected for Lorentz and polarization effects as well as for absorption (numerical). In case of the Agilent system, the program suite CrysAlis^{Pro} was used for data collection, multiscan absorption correction and data reduction.^[98] Structures were solved with direct methods using SIR97^[99] and were refined by full-matrix least-squares methods on F² with SHELXL-97.^[100] The structures were checked for higher symmetry with help of the program Platon.^[101] CCDC-989971 and , CCDC-989972 contain the supplementary crystallographic data for this paper. These data can be obtained free of charge from The Cambridge Crystallographic Data Centre via www.ccdc.cam.ac.uk/data_request/cif.

Distribution coefficients

The distribution coefficient of each complex was experimentally determined as previously reported in our group^[35] by using the “shake-flask” method. Briefly, each complex was dissolved in phosphate buffer (10 mM; pH 7.01) previously saturated with *n*-octanol to give about 1 mL of a solution with a concentration of 50 μM for

each complex. The same volume of octanol (previously saturated with 10 mM phosphate buffer) was then added and the solution was shaken 100 times and equilibrated for 4.5 h. The concentration of the complex in the aqueous phase was then evaluated by UV/Vis spectroscopy, using extinction coefficients of the complexes (Table 1). The evaluation on each complex was repeated three times.

Stability in human plasma

The stability of the compounds in human plasma at 37 °C was evaluated following a slightly modified procedure recently reported by our group.^[35] The human plasma was provided by the Blutspendezentrum, Zürich, Switzerland. Diazepam (internal standard) was obtained from Sigma–Aldrich. Stock solutions of the complexes (20 mM) and diazepam (3.2 mM) were prepared in DMSO. For a typical experiment, an aliquot of the respective stock solutions and DMSO was then added to the plasma solution (975 µL) to a total volume of 1000 µL and final concentrations of 40 µM for the complexes and diazepam. The resulting plasma solution was incubated for 48 h at 37 °C with continuous and gentle shaking (ca. 300 rpm). The reaction was stopped by addition of 2 mL of methanol, and the mixture was centrifuged for 45 min at 650 g at 4 °C. The methanolic solution was evaporated and the residue was suspended in 200 µL of 1:1 (v/v) CH₃CN/H₂O solution. The suspension was filtered and analyzed using LC-MS. A total of 40 µL of the solution was injected into the HPLC (Acquity Ultra Performance LC, Waters) that was connected to a mass spectrometer (Bruker Esquire 6000) operated in ESI mode. The Nucleodur C18 Gravity 5 µm (250 × 3 mm) reverse phase column was used with a flow rate of 0.5 mL min⁻¹ and UV absorption was measured at 300 nm. The runs were performed with a linear gradient of A (CH₃CN (Sigma Aldrich HPLC-grade)) and B (distilled water containing 0.02% TFA and 0.05% HCOOH): *t* = 0–3 min, 20% A; *t* = 7 min, 50% A; *t* = 20 min, 90% A.

DNA-binding experiments

DNA-binding constant evaluation was performed as reported previously.^[35] Briefly, DNA concentrations were evaluated by spectroscopy. The emission titrations were performed at room temperature in phosphate buffer (10 mM) with NaCl (50 mM; pH 7.01). For every sample, the Ru complex concentration was constant, between 0.6 and 8 µM, depending on the compound, and a concentrated solution of CT-DNA (type I, fibers) was added ($\epsilon_{260,CT-DNA} = 6600 \text{ M}^{-1} \text{ cm}^{-1}$ per nucleotide). After every addition, samples were incubated at room temperature for 5 min and then emission spectra were recorded (PerkinElmer Luminescence Spectrophotometer LS50B, excitation at 440 nm, excitation slit 5 nm, emission slit 10 nm, 5 averaged spectra). Additions of DNA were carried on until no further changes in spectra were observed. The DNA-binding constant (K_b) was determined by fitting the titration data to the Bard equation, as previously reported:^[35,88,102]

$$\begin{aligned} (I_a - I_f) / (I_b - I_f) &= (b - (b^2 - 2K_b^2 C [\text{DNA}] / s)^{1/2}) / 2K_b C \\ b &= 1 + K_b C + K_b [\text{DNA}] / 2s \end{aligned} \quad (1)$$

where [DNA] is the molar concentration of CT-DNA per nucleotide, I_a is the luminescence intensity of ruthenium complexes at a given DNA concentration, I_f is the luminescence intensity of complexes in the absence of DNA, I_b is the luminescence intensity of Ru com-

plexes when completely bound to DNA, C is the total Ru complex concentration, and s is the binding site size in base pairs. From plots of $(I_a - I_f) / (I_b - I_f)$ versus [DNA], K_b values were calculated by fitting the curves with OriginLab 8.6.

Singlet oxygen measurements

The singlet oxygen measurements were performed as recently reported by our group using two different methods.^[78]

Direct evaluation

Fluorescence measurements were performed on a Fluorolog-3 spectrofluorometer (Jobin Yvon Horiba, Model FL3-11) with a 450 W xenon lamp light source and single-grating excitation and emission spectrometers. For high beam intensity, the excitation slits were set to a maximum value of 29.4 nm. A colored glass filter was placed between the sample and the detector to cut off light below 695 nm. The emission signal was collected at right angle to the excitation path with an IR-sensitive liquid nitrogen cooled germanium diode detector (Edinburgh Instruments, Model EI-L). The detector was bias at -160 V. The signal-to-noise ratio of the signal detected by the Ge-diode was improved with a lock-in amplifier (Stanford Research Systems, model SR510) referenced to the chopper frequency of 126 Hz. Data acquisition was carried out with DataMax. Samples in aerated acetonitrile were prepared in a luminescence quartz cuvette with an OD = 0.2 at the irradiation wavelength. Four different transmittance filters were used to vary the intensity of the irradiation beam. Intensities of irradiation were plotted versus the areas of the singlet oxygen peaks at 1270 nm and the slope of the linear regression was calculated (S_{sample}).

Indirect evaluation

An air-saturated acetonitrile solution, containing the complex (OD = 0.1 at irradiation wavelength), *p*-nitrosodimethyl aniline (RNO; 24 µM), imidazole (12 mM) or an air-saturated PBS buffer solution, containing the complex (OD = 0.1 at irradiation wavelength), RNO (20 µM), histidine (10 mM) were irradiated in a luminescence quartz cuvette at 350 or 420 nm in a RPR100 Rayonet chamber reactor (Southern New England Ultraviolet Company) complete with twelve lamps, at different time intervals. The absorbance of the solution was then evaluated. Plots of variations in absorbance at 440 nm in PBS or at 420 nm in acetonitrile ($A_0 - A$, where A_0 is the absorbance before irradiation) versus the irradiation times for each sample were prepared and the slope of the linear regression was calculated (S_{sample}).

As a reference compound, phenalenone ($\Phi_{\text{ref}}(^1\text{O}_2) = 95\%$) was used in both methods, to obtain S_{ref} Equation (2) was applied to calculate the singlet oxygen quantum yields (Φ_{sample}) for every sample:

$$\Phi_{\text{sample}} = \Phi_{\text{ref}} * S_{\text{sample}} / S_{\text{ref}} * I_{\text{ref}} / I_{\text{sample}} \quad (2)$$

$$I = I_0 * (1 - 10^{-A_\lambda}) \quad (3)$$

I (absorbance correction factor) was obtained with Equation (3), where I_0 is the light intensity of the irradiation source in the irradiation interval and A_λ is the absorbance of the sample at wavelength λ .

Computational details

All calculations were performed employing the Gaussian 09 (G09) program^[103] together with the DFT and TD-DFT methods. The effect of functional and basis set was assessed by benchmarking their performance in the geometry and absorption properties of complex **3** for which X-ray data were available (data not shown). Four different functional (B3LYP,^[104] PBE0,^[72] CAM-B3LYP,^[105] wB97XD^[106]), four ECPs (LanL2DZ,^[107] LanL2TZ,^[107] LanL08,^[107] SDD^[73]) and four basis sets (6-31G**,^[74] 6-31+G**, 6-311G**,^[108] 6-311+G**) were tested. The PBE0/SDD/6-31G** combination was chosen as it gave the best agreement with experimental data, although the more computationally expensive PBE0/SDD/6-311G** + behaved comparably. Afterwards, geometry optimizations of complexes **2**, **3** and **6** in their ground state (GS) and lowest-lying triplet state (II-T) were performed at the PBE0/SDD/6-31G** level using the PCM solvent model.^[109] The nature of all stationary points was confirmed by normal mode analysis. For the II-T geometries the UKS method with the unrestricted PBE0 functional was adopted. The PCM model method with acetonitrile as solvent was employed to calculate eighty singlet–singlet transitions of the complexes in solution by TD-DFT.^[110] Thirty-two singlet excited states with the corresponding oscillator strengths were determined at the ground-state geometry. Similarly, eight triplet excited states were determined at the lowest-lying triplet state (II-T) geometry. A full account of all computational results is provided in the Supporting Information. Theoretical UV/Vis curves were obtained using the program GAUSSSUM 2.2.^[111] Molecular graphics images were produced using the UCSF Chimera package from the Resource for Bio-computing, Visualization, and Informatics at the University of California, San Francisco (supported by NIH P41 RR001081).^[112]

Cell culture

Human cervical carcinoma cell line (HeLa) was maintained in DMEM (Gibco) with fetal calf serum (FCS, 5%; Gibco), penicillin (100 U mL⁻¹), streptomycin (100 µg mL⁻¹) in a humidified atmosphere at 37 °C and 5% CO₂. Normal lung fibroblast cell line (MRC-5) was cultured in F-10 medium (Gibco) supplemented with FCS (10%; Gibco), penicillin (100 U mL⁻¹), streptomycin (100 µg mL⁻¹) in a humidified atmosphere at 37 °C and 5% CO₂.

Cytotoxicity studies

A fluorometric cell viability assay using resazurin (Promocell GmbH) was used to compare the cytotoxicity of the ruthenium complexes in the dark and upon UV irradiation. HeLa and MRC-5 cell lines were plated in triplicates in 96-well plates at a density of 4 × 10³ and 7.5 × 10³ cells per well in 100 µL, respectively, 24 h prior to treatment. Cells were then treated with increasing concentrations of compounds for 48 h. For phototoxicity studies, cells were treated for 4 h only with increasing concentrations of the compounds. After that, the medium was removed and replaced by fresh complete medium prior to 10 min irradiation at 350 nm (2.58 J cm⁻²) or 20 min at 420 nm (9.27 J cm⁻²). After 44 h in the incubator, the medium was replaced by 100 µL complete medium containing resazurin (0.2 mg mL⁻¹ final concentration). After 4 h incubation at 37 °C, fluorescence of the highly red fluorescent resorufin product was quantified at 590 nm emission with 540 nm excitation wavelength in a SpectraMax M5 microplate reader. Light doses were evaluated with a Gigahertz Optic X1-1 optometer.

Microscopy studies

Cellular localization of the ruthenium complexes was performed by fluorescence microscopy. HeLa cells were grown on 18 mm Menzel-gläser coverslips in 2 mL complete medium at a density of 2.5 × 10⁵ cells per mL and incubated for 2 h with the complexes at 100 µM and with 50 nm Mitotracker green FM for the last 45 min. Cells were fixed in formaldehyde solution (4% formaldehyde in PBS) and mounted on slides in Vectashield solution containing DAPI prior to viewing by confocal microscopy on a CLSM Leica SP5 microscope. The ruthenium complexes were excited at 488 nm and emission above 600 nm was recorded.

Sample preparation for HR-CS AAS

Whole-cellular fraction

Briefly, HeLa and MRC-5 cell lines were seeded in 75 cm² cell culture flask and grown until 85% confluence. The medium was then removed, the cells were washed with PBS and treated with 20 µM of the target complexes in medium for 4 h in the dark. After exposure, the medium was removed and the cells were washed with PBS and trypsinized. The pellet was collected by centrifugation at 3645 g for 5 min with a 5810R centrifuge (Eppendorf). The pellet was then redissolved in water (1 mL) and lyzed by freeze and thaw cycles and in an ultrasonic bath (20 min, VWR Ultrasonic Cleaner). An aliquot of the cell extract was used for protein quantification purposes following the Bradford method.^[113] An aliquot (120 µL) was treated with Triton X-100 (1%; 12 µL) and HCl (1 M; 12 µL) and the ruthenium content was quantified by HR-CS AAS.

Nuclear fraction

Nuclei of HeLa cells were obtained following an established procedure with minor modifications.^[114] Briefly, HeLa cells were seeded two days before treatment at a concentration of 4 × 10⁵ cells per mL in a 75 cm² cell culture flask and grown to 80% confluence and incubated with the target complexes at 20 µM for 4 h. The medium was removed, cells were washed with PBS and trypsinized. After resuspension in PBS, the pellet was collected by centrifugation (5910R, Eppendorf) at 500g for 5 min at 4 °C. The collected pellets were redissolved in 1.5 mL of lysis buffer (obtained from 1 × extraction buffer A, catalogue number E2778, Sigma–Aldrich, added 1:200 v/v Cell Lysis Solution catalogue number C1242, Sigma–Aldrich, and Protease Inhibitor Cocktail 1:500 v/v, catalogue number P8340, Sigma–Aldrich) and incubated for 15 min on ice. The samples were homogenized with a prechilled dounce homogenizer (7 mL, tight pestle A, 30 strokes) and centrifuged at 600g for 10 min at 4 °C. The supernatant was discarded and the pellets were redissolved in 2 mL of a sucrose solution (0.25 M sucrose, 10 mM MgCl₂) and layered with 2 mL of a second hypertonic sucrose solution (0.35 M sucrose, 0.5 mM MgCl₂). The suspension was centrifuged at 1450g and 4 °C for 5 min. The pellets were resuspended in the second sucrose solution (3 mL) and centrifuged at 1450g and 4 °C for 5 min to obtain the pure nuclear extract. All the steps of the isolation procedure were monitored under a phase contrast microscope on Menzel-gläser coverslips (Olympus IX81 microscope). The isolated samples were lyophilized on an Alpha 2-4 LD plus (CHRIST). The lyophilized samples were redissolved in water (1 mL); just prior to the measurements, an aliquot (20 µL) was used for protein quantification according to the Bradford method.^[91] An aliquot (120 µL) was treated with Triton X-100 (1%; 12 µL) and HCl (1 M; 12 µL) and the ruthenium content was quantified by HR-CS AAS.

HR-CS AAS measurements

AAS measurements were performed using a contrAA 700 high resolution continuum source atomic absorption spectrometer (HRCS-AAS) for the quantification of ruthenium at a wavelength of 349.8945 nm. Standards for calibration purposes were prepared as dilutions of a standard stock solution of complex **2** in a cell lysate (matrix matched calibration). For the quantification of the metal content, a volume of 25 μL was injected into the graphite tubes. Drying, pyrolysis, and atomization in the graphite furnace programs for ruthenium are presented in Table 4. The mean absorbances of duplicate injections were used throughout the study.

Step	T [$^{\circ}\text{C}$]	Ramp [$^{\circ}\text{C s}^{-1}$]	Hold [s]
drying	70	10	40
drying	85	7	30
drying	105	10	30
drying	500	50	30
pyrolysis	900	200	20
gas adaptation	900	0	5
atomization	2500	1700	8
cleaning	2600	1000	6

DNA photocleavage experiments

DNA photocleavage experiments were performed according to a method reported recently by our group.^[78] More specifically, supercoiled pcDNA3 plasmid (Invitrogen, 0.20 μg) was incubated with **1** and **2** at concentrations 1, 10, 30 and 50 μM in buffer (50 mM Tris-HCl, 18 mM NaCl, pH 7.2) then irradiated at 420 nm for 20 min (9.27 J cm^{-2}) in a RPR100 Rayonet Chamber Reactor (Southern New England Ultraviolet Company). A series of negative controls of the plasmid treated with the same concentrations of **1** and **2** in the dark was used for comparative purposes. After irradiation, gel-loading buffer (250 mg xylene cyanol in 33 mL of 150 mM Tris-HCl buffer, pH 7.6) was added to the samples and they were analyzed by electrophoresis in agarose (0.8%) in 1 \times TBE (diluted from a 10 \times solution of 108 g of Tris-HCl, and 55 g of H_3BO_3 in 900 mL of H_2O) at 70 V (Biorad Powerpack 1000, BioRad) for 2 h. The gel was stained with ethidium bromide (0.5 $\mu\text{g mL}^{-1}$), photographed and worked outanalyzed with AlphaDigiDoc 1000 CCD camera (Büchner Biotec AG) and Alphamager software. The cleavage of the target plasmid not photomediated was also studied at different incubation temperatures and in the presence of the restriction enzyme BstXI (1 h incubation at 37 $^{\circ}\text{C}$) which linearized pcDNA3 (see Chart S23 in the Supporting Information). After irradiation, gel-loading buffer (250 mg xylene cyanol in 33 mL of 150 mM Tris-HCl buffer, pH 7.6) was added to the samples and they were analyzed by electrophoresis in agarose (0.8%) in 1 \times TBE (diluted from a 10 \times solution of 108 g of Tris-HCl, and 55 g of H_3BO_3 in 900 mL of H_2O) at 70 V (Biorad Powerpack 1000, BioRad) for 2 h. The gel was prestained with ethidium bromide (0.5 $\mu\text{g mL}^{-1}$), photographed and worked outanalyzed with AlphaDigiDoc 1000 CCD camera (Büchner Biotec AG) and Alphamager software.

Acknowledgements

This work was financially supported by the Swiss National Science Foundation (Professorship N $^{\circ}$ PP00P2_133568 to G.G.),

the University of Zurich (G.G. and S.F.), the Stiftung für Wissenschaftliche Forschung of the University of Zurich (G.G. and S.F.), the Novartis Jubilee Foundation (G.G. and R.R.), the Stiftung zur Krebsbekämpfung (S.F.), the Huggenberger-Bischoff Stiftung (S.F.), the University of Zurich Priority Program (S.F.), the European COST Action (CM1105 to G.G., R.R., I.O. and L.S.), the Fonds der Chemischen Industrie (I.O.), the MC CIG Fellowship UCnanomat4iPACT grant 321791 (L.S.) and the MICINN of Spain for the Ramón y Cajal Fellowship RYC-2011-07787 and the National Plan grant CTQ2012-39315 (L.S.). The SGI/IZO-SGIker UPV/EHU is gratefully acknowledged for generous allocation of computational resources. L.S. is also grateful to Prof. J. M. Ugalde, T. Mercero and E. Ogando for their support. We thank M. Benz for X-ray data collection of compound **3**, and Dr. Jakob Heier from the Laboratory for Functional Polymers, Empa, Swiss Federal Laboratories for Material Science and Technology, for generous access to a near-IR fluorimeter. The authors thank the Center for Microscopy and Image Analysis of the University of Zurich for access to state-of-the-art equipment.

Keywords: density functional calculations · DNA binding · fluorescence microscopy · photodynamic therapy · singlet oxygen

- [1] T. J. Dougherty, C. J. Gomer, G. Jori, D. Kessel, M. Korbelik, J. Moan, Q. Peng, *J. Natl. Cancer Inst.* **1998**, *90*, 889.
- [2] D. E. J. G. Dolmans, D. Fukumura, R. K. Jain, *Nat. Rev. Cancer* **2003**, *3*, 380.
- [3] M. Triesscheijn, P. Baas, J. H. M. Schellens, F. A. Stewart, *Oncologist* **2006**, *11*, 1034.
- [4] K. Plaetzer, B. Krammer, J. Berlanda, F. Berr, T. Kiesslich, *Lasers Med. Sci.* **2009**, *24*, 259.
- [5] A. P. Castano, T. N. Demidova, M. R. Hamblin, *Photodiagn. Photodyn. Ther.* **2004**, *1*, 279.
- [6] L. M. Davids, B. Kleemann, *Cancer Treat. Rev.* **2011**, *37*, 465.
- [7] F. S. De Rosa, M. V. L. B. Bentley, *Pharm. Res.* **2000**, *17*, 1447.
- [8] B. R. Vummidi, F. Noreen, J. Alzeer, K. Moelling, N. W. Luedtke, *ACS Chem. Biol.* **2013**, *8*, 1737.
- [9] Y. Huang, G. Xu, Y. Peng, H. Lin, X. Zheng, M. Xie, *J. Ocul. Pharmacol. Ther.* **2007**, *23*, 377.
- [10] E. D. Baron, C. L. Malbasa, D. Santo-Domingo, P. Fu, J. D. Miller, K. K. Hanneman, A. H. Hsia, N. L. Oleinick, V. C. Colussi, K. D. Cooper, *Lasers Surg. Med.* **2010**, *42*, 888.
- [11] F. Dumoulin, M. Durmuş, V. Ahsen, T. Nyokong, *Coord. Chem. Rev.* **2010**, *254*, 2792.
- [12] E. S. Nyman, P. H. Hynninen, *J. Photochem. Photobiol. B* **2004**, *73*, 1.
- [13] E. Ben-Hur, W. S. Chan, in *The Porphyrin Handbook*, Vol. 19 (Eds.: K. M. Kadish, K. M. Smith, R. Guilard), Academic, Boston, **2003**, p. 1.
- [14] R. K. Pandey, G. Zheng, in *The Porphyrin Handbook*, Vol. 6 (Eds.: K. M. Kadish, K. M. Smith, R. Guilard), Academic, Boston, **2000**, p. 157.
- [15] C. Spagnul, R. Alberto, G. Gasser, S. Ferrari, V. Pierroz, A. Bergamo, T. Gianferrara, E. Alessio, *J. Inorg. Biochem.* **2013**, *122*, 57.
- [16] A. Naik, R. Rubbiani, G. Gasser, B. Spingler, *Angew. Chem.* **2014**, *126*, 7058; *Angew. Chem. Int. Ed.* **2014**, *53*, 6938.
- [17] A. Levina, A. Mitra, P. A. Lay, *Metallomics* **2009**, *1*, 458.
- [18] A. Bergamo, G. Sava, *Dalton Trans.* **2011**, *40*, 7817.
- [19] W. H. Ang, A. Casini, G. Sava, P. J. Dyson, *J. Organomet. Chem.* **2011**, *696*, 989.
- [20] N. L. Kilah, E. Meggers, *Aust. J. Chem.* **2012**, *65*, 1325.
- [21] J. M. Rademaker-Lakhai, D. van den Bongard, D. Pluim, J. H. Beijnen, J. H. M. Schellens, *Clin. Cancer Res.* **2004**, *10*, 3717.
- [22] C. G. Hartinger, S. Zorbas-Seifried, M. A. Jakupcic, B. Kynast, H. Zorbas, B. K. Keppler, *J. Inorg. Biochem.* **2006**, *100*, 891.

- [23] G. Sava, S. Zorzet, C. Turrin, F. Vita, M. Soranzo, G. Zabucchi, M. Cocchietto, A. Bergamo, S. DiGiovine, G. Pezzoni, L. Sartor, S. Garbisa, *Clin. Cancer Res.* **2003**, *9*, 1898.
- [24] C. G. Hartinger, M. A. Jakupec, S. Zorbas-Seifried, M. Groessler, A. Egger, W. Berger, H. Zorbas, P. J. Dyson, B. K. Keppler, *Chem. Biodiversity* **2008**, *5*, 2140.
- [25] N. R. Dickson, S. F. Jones, H. A. Burris, *J. Clin. Oncol.* **2011**, *29* (Suppl. Abstr. 2607).
- [26] F. Schmitt, P. Govindaswamy, G. Süß-Fink, W. H. Ang, P. J. Dyson, L. Juillierat-Jeaneret, B. Therrien, *J. Med. Chem.* **2008**, *51*, 1811.
- [27] T. Gianferrara, A. Bergamo, I. Bratsos, B. Milani, C. Spagnul, G. Sava, E. Alessio, *J. Med. Chem.* **2010**, *53*, 4678.
- [28] A. E. Friedman, J. C. Chambron, J. P. Sauvage, N. J. Turro, J. K. Barton, *J. Am. Chem. Soc.* **1990**, *112*, 4960.
- [29] M. R. Gill, J. Garcia-Lara, S. J. Foster, C. Smythe, G. Battaglia, J. A. Thomas, *Nat. Chem.* **2009**, *1*, 662.
- [30] M. R. Gill, H. Derrat, C. G. W. Smythe, G. Battaglia, J. A. Thomas, *ChemBioChem* **2011**, *12*, 877.
- [31] V. Rajendiran, M. Murali, E. Suresh, M. Palaniandavar, V. S. Periasamy, M. A. Akbarsha, *Dalton Trans.* **2008**, 2157.
- [32] W. J. Mei, N. Wang, Y. J. Liu, Y. Z. Ma, D. Y. Wang, B. X. Liang, *Transition Met. Chem.* **2008**, *33*, 499.
- [33] U. Schatzschneider, J. Niesel, I. Ott, R. Gust, H. Alborzina, S. Wölfl, *ChemMedChem* **2008**, *3*, 1104.
- [34] V. Rajendiran, M. Palaniandavar, V. S. Periasamy, M. A. Akbarsha, *J. Inorg. Biochem.* **2012**, *116*, 151.
- [35] V. Pierroz, T. Joshi, A. Leonidova, C. Mari, J. Schur, I. Ott, L. Spiccia, S. Ferrari, G. Gasser, *J. Am. Chem. Soc.* **2012**, *134*, 20376.
- [36] A. Yadav, T. Janaratne, A. Krishnan, S. S. Singhal, S. Yadav, A. S. Dayoub, D. L. Hawkins, S. Awasthi, F. M. MacDonnell, *Mol. Cancer Ther.* **2013**, *12*, 643.
- [37] T. Joshi, V. Pierroz, C. Mari, L. Gemperle, S. Ferrari, G. Gasser, *Angew. Chem.* **2014**, *126*, 3004; *Angew. Chem. Int. Ed.* **2014**, *53*, 2960.
- [38] T. Joshi, V. Pierroz, S. Ferrari, G. Gasser, *ChemMedChem* **2014**, *9*, 1419.
- [39] J. X. Zhang, J. W. Zhou, C. F. Chan, T. C. K. Lau, D. W. J. Kwong, H. L. Tam, N. K. Mak, K. L. Wong, W. K. Wong, *Bioconjugate Chem.* **2012**, *23*, 1623.
- [40] J. X. Zhang, K. L. Wong, W. K. Wong, N. K. Mak, D. W. J. Kwong, H. L. Tam, *Org. Biomol. Chem.* **2011**, *9*, 6004.
- [41] C. T. Poon, P. S. Chan, C. Man, F. L. Jiang, R. N. S. Wong, N. K. Mak, D. W. J. Kwong, S. W. Tsao, W. K. Wong, *J. Inorg. Biochem.* **2010**, *104*, 62.
- [42] Y. Sun, L. E. Joyce, N. M. Dickson, C. Turro, *Chem. Commun.* **2010**, *46*, 2426.
- [43] F. Gao, H. Chao, Y. F. Wei, Y. X. Yuan, B. Peng, X. Chen, K. C. Zheng, L. N. Ji, *Helv. Chim. Acta* **2008**, *91*, 395.
- [44] S. P. Foxon, C. Green, M. G. Walker, A. Wragg, H. Adams, J. A. Weinstein, S. C. Parker, A. J. H. M. Meijer, J. A. Thomas, *Inorg. Chem.* **2012**, *51*, 463.
- [45] H. J. Yu, H. Chao, L. Jiang, L. Y. Li, S. M. Huang, L. N. Ji, *Inorg. Chem. Commun.* **2008**, *11*, 553.
- [46] F. Gao, H. Chao, F. Zhou, Y. X. Yuan, B. Peng, L. N. Ji, *J. Inorg. Biochem.* **2006**, *100*, 1487.
- [47] H. J. Yu, S. M. Huang, L. Y. Li, H. N. Jia, H. Chao, Z. W. Mao, J. Z. Liu, L. N. Ji, *J. Inorg. Biochem.* **2009**, *103*, 881.
- [48] X. L. Zhao, Y. Z. Ma, K. Z. Wang, *J. Inorg. Biochem.* **2012**, *113*, 66.
- [49] H. Y. Ding, X. S. Wang, L. Q. Song, J. R. Chen, J. H. Yu, L. Chao, B. W. Zhang, *J. Photochem. Photobiol. A* **2006**, *177*, 286.
- [50] S. P. Foxon, M. A. H. Alamiry, M. G. Walker, A. J. H. M. Meijer, I. V. Sazanovich, J. A. Weinstein, J. A. Thomas, *J. Phys. Chem. A* **2009**, *113*, 12754.
- [51] A. Hergueta-Bravo, M. E. Jiménez-Hernández, F. Montero, E. Oliveros, G. Orellana, *J. Phys. Chem. B* **2002**, *106*, 4010.
- [52] X. W. Liu, Y. M. Shen, J. L. Lu, Y. D. Chen, L. Li, D. S. Zhang, *Spectrochim. Acta Part A* **2010**, *77*, 522.
- [53] X. W. Liu, Y. D. Chen, L. Li, J. L. Lu, D. S. Zhang, *Spectrochim. Acta Part A* **2012**, *86*, 554.
- [54] G. Shi, S. Monro, R. Hennigar, J. Colpitts, J. Fong, K. Kasimova, H. Yin, R. DeCoste, C. Spencer, L. Chamberlain, A. Mandel, L. Lilge, S. A. McFarland, *Coord. Chem. Rev.* DOI: 10.1016/j.ccr.2014.04.012.
- [55] A. M. Angeles-Boza, P. M. Bradley, P. K. L. Fu, S. E. Wicke, J. Bacsá, K. R. Dunbar, C. Turro, *Inorg. Chem.* **2004**, *43*, 8510.
- [56] B. Maity, M. Roy, B. Banik, R. Majumdar, R. R. Dighe, A. R. Chakravarty, *Organometallics* **2010**, *29*, 3632.
- [57] S. Monro, J. Scott, A. Chouai, R. Lincoln, R. Zong, R. P. Thummel, S. A. McFarland, *Inorg. Chem.* **2010**, *49*, 2889.
- [58] C. S. Choi, L. Mishra, T. Mutai, K. Araki, *Bull. Chem. Soc. Jpn.* **2000**, *73*, 2051.
- [59] A. Kleineweischede, J. Mattay, *J. Organomet. Chem.* **2006**, *691*, 1834.
- [60] X. Chen, F. Gao, W. Y. Yang, J. Sun, Z. X. Zhou, L. N. Ji, *Inorg. Chim. Acta* **2011**, *378*, 140.
- [61] J. Etedgui, Y. Diskin-Posner, L. Weiner, R. Neumann, *J. Am. Chem. Soc.* **2011**, *133*, 188.
- [62] Y. Sun, D. A. Lutterman, C. Turro, *Inorg. Chem.* **2008**, *47*, 6427.
- [63] M. Li, P. Lincoln, *J. Inorg. Biochem.* **2009**, *103*, 963.
- [64] J. Rusanova, S. Decurtins, E. Rusanov, H. Stoeckli-Evans, S. Delahaye, A. Hauser, *J. Chem. Soc. Dalton Trans.* **2002**, 4318.
- [65] N. Nickita, G. Gasser, P. Pearson, M. J. Belousoff, L. Y. Goh, A. M. Bond, G. B. Deacon, L. Spiccia, *Inorg. Chem.* **2009**, *48*, 68.
- [66] S. Dalton, S. Glazier, B. Leung, S. Win, C. Megatalski, S. Burgmayer, *J. Biol. Inorg. Chem.* **2008**, *13*, 1133.
- [67] S. Fantacci, F. De Angelis, A. Sgamellotti, N. Re, *Chem. Phys. Lett.* **2004**, *396*, 43.
- [68] L. C. Xu, J. Li, Y. Shen, K. C. Zheng, L. N. Ji, *J. Phys. Chem. A* **2007**, *111*, 273.
- [69] H. Ishida, S. Tobita, Y. Hasegawa, R. Katoh, K. Nozaki, *Coord. Chem. Rev.* **2010**, *254*, 2449.
- [70] E. Amouyal, A. Homsí, J. C. Chambron, J. P. Sauvage, *J. Chem. Soc. Dalton Trans.* **1990**, 1841.
- [71] Y. Jenkins, A. E. Friedman, N. J. Turro, J. K. Barton, *Biochemistry* **1992**, *31*, 10809.
- [72] J. P. Perdew, K. Burke, M. Ernzerhof, *Phys. Rev. Lett.* **1996**, *77*, 3865.
- [73] P. Fuentealba, H. Preuss, H. Stoll, L. Von Szentpály, *Chem. Phys. Lett.* **1982**, *89*, 418.
- [74] R. Ditchfield, W. J. Hehre, J. A. Pople, *J. Chem. Phys.* **1971**, *54*, 724.
- [75] D. Jacquemin, E. Brémond, A. Planchat, I. Ciofini, C. Adamo, *J. Chem. Theory Comput.* **2011**, *7*, 1882.
- [76] T. Österman, M. Abrahamsson, H. C. Becker, L. Hammarström, P. Persson, *J. Phys. Chem. A* **2012**, *116*, 1041.
- [77] N. J. Farrer, J. A. Woods, V. P. Munk, F. S. Mackay, P. J. Sadler, *Chem. Res. Toxicol.* **2010**, *23*, 413.
- [78] A. Leonidova, V. Pierroz, R. Rubbiani, J. Heier, S. Ferrari, G. Gasser, *Dalton Trans.* **2014**, *43*, 4287.
- [79] N. Ueberschaar, H. M. Dahse, T. Bretschneider, C. Hertweck, *Angew. Chem.* **2013**, *125*, 6305; *Angew. Chem. Int. Ed.* **2013**, *52*, 6185.
- [80] I. Kraljić, S. El Mohsni, *Photochem. Photobiol.* **1978**, *28*, 577.
- [81] I. E. Kochevar, R. W. Redmond, H. S. Lester Packer, in *Methods in Enzymology, Vol. 319*, Academic, **2000**, p. 20.
- [82] W. Spiller, H. Kliesch, D. Woehrlé, S. Hackbarth, B. Roeder, G. Schnurpfeil, *J. Porphyrins Phthalocyanines* **1998**, *02*, 145.
- [83] R. Schmidt, C. Tanielian, R. Dunsbach, C. Wolff, *J. Photochem. Photobiol. A* **1994**, *79*, 11.
- [84] M. Ochsner, *J. Photochem. Photobiol. B* **1997**, *39*, 1.
- [85] B. M. Zeglis, V. C. Pierre, J. K. Barton, *Chem. Commun.* **2007**, 4565.
- [86] A. M. Pyle, J. P. Rehmman, R. Meshoyrer, C. V. Kumar, N. J. Turro, J. K. Barton, *J. Am. Chem. Soc.* **1989**, *111*, 3051.
- [87] V. Fernández-Moreira, F. L. Thorp-Greenwood, M. P. Coogan, *Chem. Commun.* **2010**, *46*, 186.
- [88] M. T. Carter, M. Rodriguez, A. J. Bard, *J. Am. Chem. Soc.* **1989**, *111*, 8901.
- [89] E. Delaey, F. van Laar, D. De Vos, A. Kamuhabwa, P. Jacobs, P. de Witte, *J. Photochem. Photobiol. B* **2000**, *55*, 27.
- [90] L. Oehninger, M. Stefanopoulou, H. Alborzina, J. Schur, S. Ludewig, K. Namikawa, A. Munoz-Castro, R. W. Koster, K. Baumann, S. Wölfl, W. S. Sheldrick, I. Ott, *Dalton Trans.* **2013**, *42*, 1657.
- [91] M. M. Bradford, *Anal. Biochem.* **1976**, *72*, 248.
- [92] G. Gasser, S. Neumann, I. Ott, M. Seitz, R. Heumann, N. Metzler-Nolte, *Eur. J. Inorg. Chem.* **2011**, 5471.
- [93] B. Armitage, *Chem. Rev.* **1998**, *98*, 1171.
- [94] M. B. Fleisher, K. C. Waterman, N. J. Turro, J. K. Barton, *Inorg. Chem.* **1986**, *25*, 3549.
- [95] J. K. Barton, A. L. Raphael, *J. Am. Chem. Soc.* **1984**, *106*, 2466.
- [96] A. Leonidova, V. Pierroz, R. Rubbiani, Y. Lan, A. G. Schmitz, A. Kaech, R. K. O. Sigel, S. Ferrari, G. Gasser, *Chem. Sci.* **2014**, DOI: 10.1039/C3SC53550A.
- [97] STOE-IPDS Software package X-Area, Vers. 1.38 ed., **2006**.

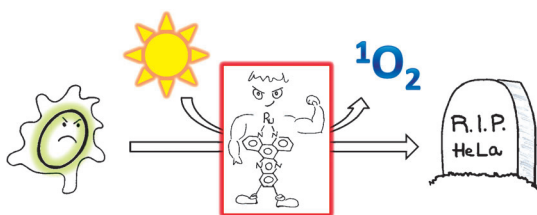
- [98] CrysAlisPro, Vers. 171.36, Agilent Technologies, Xcalibur CCD system, Oxford, UK, 2011.
- [99] A. Altomare, M. C. Burla, M. Camalli, G. L. Cascarano, C. Giacovazzo, A. Guagliardi, A. G. G. Moliterni, G. Polidori, R. Spagna, *J. Appl. Crystallogr.* **1999**, 32, 115.
- [100] G. M. Sheldrick, *Acta Crystallogr.* **2008**, A64, 112.
- [101] A. L. Spek, *J. Appl. Crystallogr.* **2003**, 36, 7.
- [102] W. A. Kalsbeck, H. H. Thorp, *J. Am. Chem. Soc.* **1993**, 115, 7146.
- [103] Gaussian 09, Revision B.01, M. J. Frisch, G. W. Trucks, H. B. Schlegel, G. E. Scuseria, M. A. Robb, J. R. Cheeseman, G. Scalmani, V. Barone, B. Mennucci, G. A. Petersson, H. Nakatsuji, M. Caricato, X. Li, H. P. Hratchian, A. F. Izmaylov, J. Bloino, G. Zheng, J. L. Sonnenberg, M. Hada, M. Ehara, K. Toyota, R. Fukuda, J. Hasegawa, M. Ishida, T. Nakajima, Y. Honda, O. Kitao, H. Nakai, T. Vreven, J. A. J. Montgomery, J. E. Peralta, F. Ogliaro, M. Bearpark, J. J. Heyd, E. Brothers, K. N. Kudin, V. N. Staroverov, R. Kobayashi, J. Normand, K. Raghavachari, A. Rendell, J. C. Burant, S. S. Iyengar, J. Tomasi, M. Cossi, N. Rega, J. M. Millam, M. Klene, J. E. Knox, J. B. Cross, V. Bakken, C. Adamo, J. Jaramillo, R. Gomperts, R. E. Stratmann, O. Yazyev, A. J. Austin, R. Cammi, C. Pomelli, J. W. Ochterski, R. L. Martin, K. Morokuma, V. G. Zakrzewski, G. A. Voth, P. Salvador, J. J. Dannenberg, S. Dapprich, A. D. Daniels, Ö. Farkas, J. B. Foresman, J. V. Ortiz, J. Cioslowski, D. J. Fox, Gaussian, Inc. Wallingford CT, 2009.
- [104] A. D. Becke, *J. Chem. Phys.* **1993**, 98, 5648.
- [105] T. Yanai, D. P. Tew, N. C. Handy, *Chem. Phys. Lett.* **2004**, 393, 51.
- [106] J. D. Chai, M. Head-Gordon, *Phys. Chem. Chem. Phys.* **2008**, 10, 6615.
- [107] P. J. Hay, W. R. Wadt, *J. Chem. Phys.* **1985**, 82, 270.
- [108] A. D. McLean, G. S. Chandler, *J. Chem. Phys.* **1980**, 72, 5639.
- [109] D. M. York, M. Karplus, *J. Phys. Chem. A* **1999**, 103, 11060.
- [110] G. Scalmani, M. J. Frisch, B. Mennucci, J. Tomasi, R. Cammi, V. Barone, *J. Chem. Phys.* **2006**, 124, 094107.
- [111] N. M. O'Boyle, A. L. Tenderholt, K. M. Langner, *J. Comput. Chem.* **2008**, 29, 839.
- [112] E. F. Pettersen, T. D. Goddard, C. C. Huang, G. S. Couch, D. M. Greenblatt, E. C. Meng, T. E. Ferrin, *J. Comput. Chem.* **2004**, 25, 1605.
- [113] M. M. Bradford, *Anal. Biochem.* **1976**, 72, 248.
- [114] M. Muramatsu, K. Smetana, H. Busch, *Cancer Res.* **1963**, 23, 510.

Received: March 27, 2014

Revised: July 10, 2014

Published online on ■ ■ ■, 0000

FULL PAPER



Fear the reaper: Six Ru^{II} polypyridyl complexes were fully characterized and evaluated as potential photosensitizers for photodynamic therapy applications. Two displayed impressive phototoxic activity upon irradiation at 420 nm and ex-

tremely competitive phototoxic indexes. The good cellular uptake, together with preferential nuclear accumulation and very efficient light induced DNA cleavage suggest a DNA-based mode of phototoxic action.

Photodynamic Therapy

*C. Mari, V. Pierroz, R. Rubbiani, M. Patra, J. Hess, B. Spingler, L. Oehninger, J. Schur, I. Ott, L. Salassa, S. Ferrari, G. Gasser**

**DNA Intercalating Ru^{II} Polypyridyl Complexes as Effective Photosensitizers in Photodynamic Therapy**